STRESS RELAXATION MODELING OF COMPOSITE POROUS SCAFFOLDS

By

RAHUL MIRANI

Bachelor of Engineering in Chemical Engineering

Nirma Institute of Technology

Ahmedabad, Gujarat, India

2006

Submitted to the Faculty of the
Graduate College of the
Oklahoma State University
in partial fulfillment of
the requirements for
the Degree of
MASTER OF SCIENCE
December, 2009

STRESS RELAXATION MODELING OF COMPOSITE

POROUS SCAFFOLDS

Thesis Approved:

Dr. Sundararajan V. Madihally

Thesis Adviser

Dr. Russell R. Rhinehart

Dr. Arland Johannes

Dr A. Gordon Emslie

Dean of the Graduate College

ACKNOWLEDGMENTS

I would like to place on record my sincere gratitude and thanks to Dr. Sundar Madihally, my Advisor, for the guidance, suggestions, enthusiasm and encouragement he provided in my research work. I am also indebted to him for the financial support he extended during my stay at Oklahoma State University. I will cherish the knowledge he imparted to me and hope that I will be able to make good use of it in my future endeavors.

I would like to thank Dr. Russell R. Rhinehart and Dr. Arland H. Johannes for being in my thesis advisory committee and for the help I received from them in completing my thesis. Special thanks to Jonathan Pratt, a senior in the department, for helping out with the etching process and to Prithwijit Ghoshal, for his help with the optimization. My fellow lab mates, Dr. Benjamin Lawrence, Pooja Iyer, Seok Won Pok, Jong Kyu Hong, Dhananjay Dhane and Kornkarn for all their help and support. I also acknowledge the help rendered by the faculty and staff of the department of Chemical Engineering at Oklahoma State University.

TABLE OF CONTENTS

Chapter Page

LIST OF TABLES

LIST OF FIGURES

CHAPTER I

INTRODUCTION

Using biodegradable scaffolds that can support and guide the in-growth of cells have been a promising solution to regenerate tissue parts. Scaffolds generated from natural [1] and synthetic polymers or after removing the cellular components from xenogeneic tissues [2] have been used for this purpose. Since naturally formed matrices such as Small Intestinal Sub mucosa (SIS) are constrained by large-scale preparations of reliable, and reproducible products [3], forming synthetic matrices from biodegradable polymers such as poly(glycolic acid) (PGA), poly(lactic acid) (PLA), polycaprolactone (PCL), poly(lactic-co-glycolic acid) (PLGA), gelatin, chitosan and glycosaminoglycans have been explored in forming scaffolds [4, 5]. However, the dearth of biomaterials that could form scaffolds eliciting controlled cellular responses with essential mechanical properties has necessitated search for novel biomaterials. As a solution to this impending problem, blending two or more polymers is a good option to develop scaffolds with wide range of physicochemical properties and cellular interactions [4, 6-9]. A reliable method to develop scaffolds is to blend individual polymeric structures by the process of controlled rate freezing and freeze drying [10]. In this configuration, the desired properties of the individual polymeric structures is harnessed and contributed towards the composite scaffold structure as whole. Also, the mechanical and degradation properties are tailored by selecting appropriate synthetic polymers.

Mechanical properties of synthetic scaffolds have been quantified by either tensile testing or compression testing. However, many parts of the body and the tissue structures within the body part are exposed to different kinds of stresses namely tensile, compressive, cyclical, and flexural stresses. Many biomechanical analyses to understand the force distribution and stress propagation have revealed that majority of the tissues [11] behave as viscoelastic materials rather than pure elastic materials typically observed in engineering applications [12]. Viscoelastic materials store and dissipate energy within the complex molecular structure; producing hysteresis and allowing creep and stress relaxation to occur. They are found to display time-dependent and load-history-dependent mechanical behavior, are nearly incompressible, undergo large deformations, and display nonlinear material behavior [13-17] and are anisotropic [18-21]. Hence, analyzing viscoelastic properties of synthetic scaffolds is critical for utilization in tissue engineering and future design of novel biomaterials to be used in tissue regeneration applications [22]. Further, one has to perform viscoelastic testing comparing it to properties that native tissues possess to identify the utility and the quality of the regenerated tissue. Interestingly, very few studies have been performed to understand the viscoelastic nature of porous structures used in tissue regeneration [23].

The objective of this study was evaluating the viscoelastic characteristics of potential scaffolds to be used in tissue regeneration. PLGA based composite scaffold was used as a model structure for evaluating viscoelastic stress relaxation characteristics. Quasi Linear Viscoelastic (QLV) model, the most widely used model in biomechanics, was used to quantify the viscoelastic behavior in terms of the physiological model parameters. This study is grouped into the following two specific aims.

SPECIFIC AIM I: Evaluation of viscoelastic characteristics of porous scaffolds.

First, composite scaffolds were formed using PLGA and chitosan-gelatin. PLGA membranes were also etched to form nanoscale features to facilitate easy spreading of chitosan-gelatin. Viscoelastic "Ramp-and-Hold" tests were performed to assess the stress relaxation properties of the scaffolds. Load limits were determined by constant rate uniaxial tensile test. Viscoelastic "Ramp-and-Hold" stress relaxation tests consist of a *loading phase* where the sample is subjected to a constant rate of loading for a specific value of percentage strain followed by holding the sample at the strain at the end of the loading phase for a specific duration, which is the *relaxation phase.* To understand the effect of variable loading rate, temperature and relaxation times, experiments were performed under the following conditions:

a) Two different strain rates of 3.125 % s^{-1} and 12.5 % s^{-1}
b) Two different values of relaxation times were used (60s, and 100s), and
c) Two different environmental temperatures (25°C and 37°C) in hydrated conditions.

It was observed from the results that the relaxation of PLGA based structures was sensitive to the temperature but not so to the rate of loading and the relaxation time. Peak stresses were higher in magnitude at 25°C than at 37°C.

SPECIFIC AIM II: Analysis of stress relaxation by Quasi Linear Viscoelastic model.

The most commonly used model in bioengineering is the QLV model, introduced by Fung [24] and later modified by many others [25-31]. The viscoelastic stress relaxation characteristics of the PLGA composite were evaluated using QLV model. The integral term encountered in the equation for the output stress was solved analytically to obtain two separate equations, one for the loading part and the other for the relaxation part of the experiment. The five constant parameters of the model A, B, C, τ_1, τ_2 were regressed by simultaneous minimization of the Sum Squared Error (SSE) as the objective function for the loading and relaxation experimental data using a cyclic search heuristic algorithm. To ensure global convergence of the regression algorithm the optimizer incorporated the rule of "Best-of-N" [32]. This allowed the optimizer to start from N number of random initial guesses to probably achieve a global minimum value for the objective function. The optimization also used a novel steady state stopping criterion [33]. Experimentally obtained values for the untreated PLGA, the treated PLGA and the composite PLGA scaffolds were regressed and optimized to understand the difference in their viscoelastic behavior. Also, the viscoelastic characteristics of the composite scaffold were evaluated in tandem with the natural matrix SIS. Results of evaluating the model parameters and normalized output stress plots show that the PLGA scaffolds relax better than SIS.

CHAPTER II

BACKGROUND

2.1. Emergence of Tissue Engineering:

Tissue engineering is an interdisciplinary field combining the knowledge of engineering and life science towards the development of biological substitutes that restores, maintains, or enhances tissue and organ function or a whole organ [34]. The seeds of tissue engineering were laid in the early 1970's when Dr. W.T. Green, a pediatric orthopedic surgeon in Boston, performed experiments to generate new cartilage by seeding chondrocytes onto spicules of bone, implanted in nude mice. His effort although, unsuccessful, paved the way for Drs. John Burke and Ioannis Yannas who worked to generate a tissue-engineered skin substitute using a collagen matrix to support the growth of dermal fibroblasts [35]. It was only in 1988 through the efforts of Dr. Robert Langer and many others who coined the word tissue engineering. The idea of using synthetic biocompatible/biodegradable polymers configured as scaffolds also gained prominence for seeding cells, in contrast to the predominant use of naturally occurring scaffolds. Naturally occurring scaffolds have variations in physical and chemical properties that cannot be manipulated, which results in unpredictable outcomes.

According to the United Network for Organ Sharing (UNOS) statistics [36], the number of patients on the waiting list for an organ transplant in the United States is 100,832. Only 25,625 transplants have been performed and the number of available donors is only 12,931. Thousands of patients die every year waiting for an organ transplant. Tissue engineering with its ability to conjure up a whole organ in the laboratory is seen as a highly possible solution. This, however, is the short term goal. The potential impact of this field is far broader. Synthetically engineered tissues, in vitro, could greatly accelerate the development of new drugs that may cure patients, thus greatly reducing the need for organ transplant [37].

2.2. Tissue Engineering Basics:

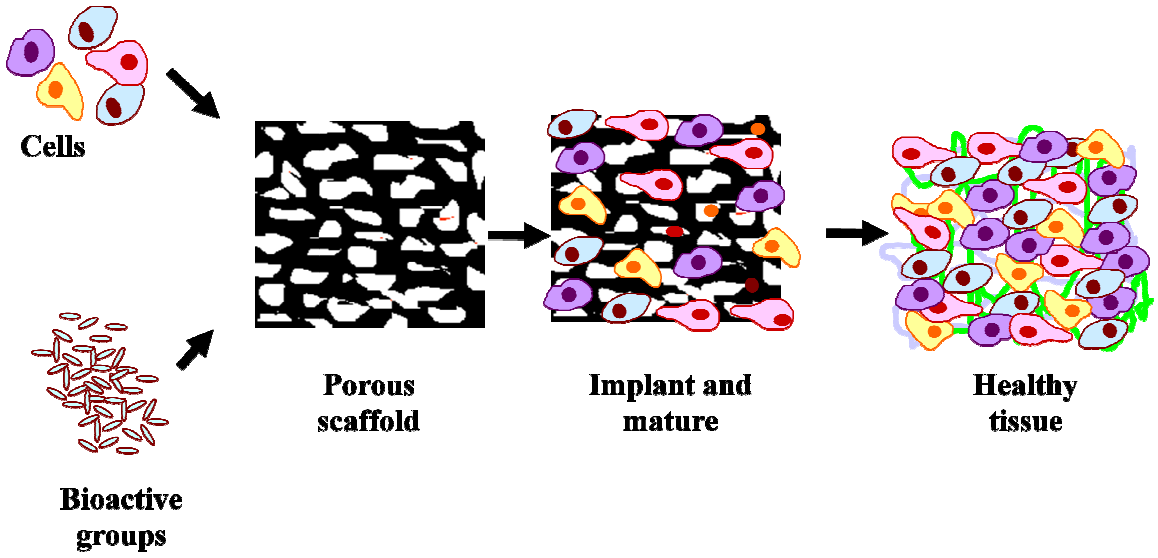

Figure 1: A typical procedure to develop a healthy tissue, in-vitro, through tissue engineering

According to the typical tissue engineering approach **(Figure 1)**, first the cells are collected from a medical biopsy. These cells are expanded in number by culturing in a growth medium or culture medium, consisting of essential nutrients for populating cells.

The expanded cells are then seeded onto synthetic/natural porous biodegradable and biocompatible matrices called as “scaffolds”. Suitable growth factors and bioactive groups are supplied for cellular growth and the cells are allowed to mature. This process of supplying the cells with nutrients is carried out in a bioreactor which facilitates cell multiplication that fills the scaffold with tissue and allows the cells to grow. The construct is transferred to the human body and the scaffold integrates concomitantly supporting body functions. Over time, as the cells proliferate the scaffold biodegrades, gradually allowing blood vessels and growth factors to make contact with the cells. Through this process, the scaffold further biodegrades while the cells proliferate and differentiate into the desired tissue.

2.3. Tissue Engineering Scaffolds:

Cells are implanted onto porous, 3-D structures capable of supporting tissue formation, often called as scaffolds. They usually serve many functions including i) cells adhesion and migration, ii) enable transport of vital nutrients and iii) exert mechanical and biological influences to modify cellular behavior. To achieve the goal of tissue regeneration the scaffold used must be biocompatible so that it is not rejected by the body; biodegradable so that it is absorbed by the surrounding tissues; should have adequate pore size necessary for cell colonization and transport of nutrients for cellular growth. The most important feature that the scaffold must possess is the mechanical strength to endure the stresses that the native tissues are exposed to. Every tissue in the human body is structured according to the function it performs. In order to design novel biomaterials, it becomes necessary to understand the mechanical environment and structural requirement of these different tissues.

2.3.1. Native Tissues; types and structure: Different tissues found in the human body have structures that are specific to their functions. The various functions in the body like breathing, digestion, excretion, and vision are performed by organs like the heart, lungs, small and large intestines, the urinary bladder, and eyes. For example, the heart performs the function of pumping blood to and from the other organs in the body. It contains muscle tissues that help it do so. Heart also contains fibrous tissue structures that make up the heart valves and other special tissues that help it regulate the rhythmic beating [38]. These tissues display nonlinear elastic and viscoelastic characteristics [39]. Also, the human skin is a nonlinearly viscoelastic material. The elastic coefficient for the skin is very low (~0.000057 MPa) compared to some other tissue structures in the body [39]. The bone, a connective tissue is subjected to constant compressive and shear type of stresses and is modeled as a linear elastic material [40, 41]. The cartilage, another example of connective tissue is described as a linear [42, 43], quasilinear [44, 45], and nonlinear [46] viscoelastic material [47]. Majority of the tissue structures in the body are found to be viscoelastic. Hence it is necessary to assess or understand the viscoelastic characteristics of materials used as scaffolds for tissue engineering applications.

Small Intestinal Sub mucosa (SIS), isolated from the intestines of bovine after removing the mucosal, serosal and muscular layers of the intestine is one natural scaffold that has been successfully used in tissue engineering applications. It has been used clinically for multiple types of hernia repair [48, 49], wound healing [50], bladder augmentation [51] to name a few. It is, however, constrained by production of a large set of similar samples. Thus the outcome of using SIS as a tissue engineering scaffold cannot be predicted with the highest of the confidence. As a result, forming synthetic scaffolds

using natural and synthetic polymers or a mixture of both is considered to be an attractive alternative [52, 53].

2.3.2. Methodology of forming scaffolds: A plethora of fabrication techniques are available for generating tissue engineering scaffolds. Each technique has its advantages, but none can be considered as an ideal method of scaffold fabrication. The choice of fabrication technique is dependent on the structure and properties of the native tissue that is to be regenerated. Some of the strategies are Solvent Casting and Particulate Leaching (SCPL) [54, 55], gas foaming [56], 3D printing [57, 58], electro spinning [59], and freeze-drying [60].

Solvent Casting and Particulate Leaching technique makes use of porogen particles like sodium chloride, gelatin sphere or paraffin spheres to porous scaffolds with regular porosity and with limited thickness. In this method of scaffold formation first the polymer is dissolved in a soluble organic solvent and the resultant polymer solution is cast in molds filled with porogen particles. The solvent is then allowed to evaporate by air drying. The remaining composite structure in the mold is then immersed in a bath of liquid suitable to dissolve the porogen to from the porous scaffold. A major drawback of the SCPL technique lies in the use of organic solvents which must be fully removed to avoid damage to cells seeded on the scaffold. [61].

The technique of gas foaming eliminated the use of organic solvents for forming porous scaffolds from polymers by using a gas porogen instead of a solid porogen as in the case of SCPL technique. In this method, first a disc shaped structure is made from the desired polymer by the process of compression molding. These discs are then exposed to high

pressure carbon dioxide for several days which results in the formation of a sponge like structure [61].

3D printing also called Computer-aided Design (CAD) and Computer-aided Manufacturing (CAM) method uses the CAD software to design a three-dimensional structure and then the scaffold is generated by using ink-jet printing using the desired polymer melt. The advantage of this method over the others is that porosity and the pore size of the scaffold can be altered and controlled according to the user's choice [61].

The process of controlled rate of freezing and freeze-drying is the fastest and the most commonly used method of formation of porous structures from polymers. In this method the polymers is first dissolved in a suitable solvent and then water is added to this polymer solution. The two liquids are then mixed to obtain an emulsion. This emulsion is then frozen either by keeping in a freezer for a specific amount of time or by dipping in liquid nitrogen. This causes the water to freeze and form crystals. The frozen emulsion is then freeze-dried in a lyophilizer to remove the dispersed water and solvent, leaving behind a solidified, porous polymeric structure.

Scaffold structures formed using natural polymers like gelatin, chitosan, glycosaminoglycans support cell growth but are mechanically weak in bearing the stresses experienced by body tissues [62]. Blending two polymers is an option to develop scaffolds with wide range of physicochemical properties and cellular interactions [4, 6-9]. The strategy is to use a synthetic and natural polymer mixture harnessing the properties of both to form a composite structure. In this configuration, the mechanical and degradation properties can be tailored by selecting appropriate synthetic polymers. The

method of controlled rate freezing and freeze-drying is adopted to form the composite structure made of gelatin-chitosan reinforced by a central layer of PLGA similar to that reported by Lawrence et *al.*, [10]. The composite is designed to mimic the biological properties, tensile properties and degradation characteristics of SIS.

PLGA is a copolymer of two monomers, glycolic acid and lactic acid. It degrades as a result of hydrolysis in the presence of water to produce the original monomers, lactic acid and glycolic acid, which are by-products of various metabolic pathways in the body. Hence the body can effectively deal with the two monomers. It is available in different forms like the 50:50 PLGA which is a composition of 50% lactic acid and 50% glycolic acid. Likewise 75:25 PLGA is composed of 75% lactic acid and 25% glycolic acid. The PLGA made using a 50:50 monomer ratio exhibits the fastest degradation rate of all the available configurations.(about two months) [10].

Chitosan is used to account for the porous structure necessary for cell seeding and growth. It is, however, very brittle with a break strain of 40-50% under hydrated conditions [62]. Other disadvantages like the limited cell growth characteristic and the dependence of degradation time on the degree of deacetylation (DD) and pH have been recognized [63]. Hence in order to improve upon the shortcomings of chitosan, it is blended with gelatin and a mixture of gelatin-chitosan is used to form the porous structure instead [63]. Gelatin improves the biological activity of chitosan as it contains Arg-Gly-Asp (RGD) like sequence that promotes cell adhesion and migration. Gelatin-chitosan scaffolds have been explored previously in regeneration of various tissues [64], cartilage [65] and bone.

2.4. Mechanical Analysis:

Majority of the studies in tissue engineering concerning scaffold materials are focused on cell culture studies, measuring porosity and understanding the degradation characteristics of scaffolds. However, recent advances have shown that the physical properties of the scaffold such as pore size, and void fraction provide cues to guide cell colonization [66], apart from chemical properties such as cell-binding sites necessary for cell attachment. Surface features such as edges, grooves, and roughness also influence cell behavior [67, 68]. Cells from various origins react very differently to changes in architectures, such as pore features and topographies [68, 69]. Cellular activity is also influenced by stiffness of the scaffold material [70-72]. These properties can be investigated only by conducting exhaustive mechanical testing of the material under consideration.

Although cell culture studies and degradation characteristics of scaffolds are important to determine the utility of a matrix in tissue engineering, careful mechanical analysis is important. As explained in the earlier sections that the tissues in the human body possess mechanical characteristic depending on their location and the function they perform. An artificial scaffold such as the PLGA composite must possess mechanical characteristics similar to the native tissues so as to successfully achieve the goal of tissue regeneration.

Typical mechanical analysis of synthetic tissue engineering scaffolds is limited to performing tensile, compressive and cyclic tests.

Tensile test: Also called a tension test is the preliminary mechanical analysis that can be performed on a material. It consists basically pulling a material under a constant applied load at a constant rate of extension till the material breaks or fails.

If a tissue structure “snaps back” to its initial neutral state (dimensions, internal structure, etc.), immediately, as the externally imposed stress or strain is removed, the structure is termed *elastic*. For elastic materials, the stress-strain plot displays linear behavior and the material is said to obey the “Hooke’s law”. The ratio of stress to strain is a constant called as the Elastic Modulus or Young’s Modulus, E, which represents the slope. The Elastic Modulus is a measure of stiffness of the material. One common example of an elastic material is a rubber band which returns to its original shape after it is stretched and released.

At the point that the curve is no longer linear, Hooke’s law is not applicable and the material undergoes permanent deformation. This point is called the elastic or proportionality limit. From this point onwards in the test, the material reacts plastically to any further increase in the stress/load. This region is the region of plastic deformation, which means that the material will no longer return to its original unstressed position once the stress/load is removed. A common example of such a material is Polyether Terepthalate [73].

Compression test: A compression test determines behavior of a material under compressive loads. The specimen is compressed and deformation at various loads is recorded. Compressive stress and strain curves are useful in determining elastic limit, proportionality limit, yield strength and compressive strength [74]. Many biological tissues like the cartilage in the knee are subjected to compressive loads in day to day activities and hence compressive testing is essential to understand the behavior and the performance of these tissues under the applicable loads.

Cyclic test: Normal, everyday movements like walking, swinging of the arms, lifting loads are repetitive in nature. Hence, the assessment of the tissue mechanical behavior in such cases requires conducting a cyclical test [25]. In this testing procedure the sample is loaded to a predetermined amount of peak stress and then the stress is removed. Several such cycles of the loading and unloading type are followed consecutively one after the other.

The methods described above are the preliminary methods to gauge the mechanical properties and do not sufficiently describe the material behavior. Also, as majority of the tissue structures in the body display viscoelastic characteristics it is necessary to assess the viscoelastic properties of the synthetic polymeric scaffolds.

2.5. Viscoelasticity:

Most biological tissues display time dependent and load-history-dependent mechanical behavior. Soft tissues such as muscles, tendons, ligaments, fascia, nerves, fibrous tissues, fat, blood vessels and synovial membranes are incompressible or nearly so, undergo large deformations, and display nonlinear material behavior [13-17]. They are found to exhibit viscoelastic character rather than pure elastic material behavior [12], and are anisotropic [18-21]. Further, porous polymeric biodegradable structures utilized in tissue regeneration also show viscoelastic behavior [26, 75]. Viscoelasticity is the property of the material that exhibits both viscous and elastic characteristic while undergoing deformation. Viscoelastic materials store and dissipate energy within the complex molecular structure; producing hysteresis and allowing creep and stress relaxation to occur. Hence, a full description of the mechanical response of materials requires

deciphering the viscoelasticity. Interestingly, very few studies have been performed to understand the viscoelasticity of scaffolds used in tissue regeneration [23].

As mentioned earlier hysteresis, stress relaxation and creep are characteristics of viscoelastic materials. Hysteresis can be explained as the phase lag associated with a dissipation of mechanical energy observed in the stress strain relationship of a material under the influence of loading and unloading cycles.

Stress relaxation is the behavior of a material under the effect of an applied constant rate of strain over a period of time followed by holding the material at this strain. The output stress reaches a peak under the influence of the applied constant rate of strain and then relaxes over time during the hold period.

Creep is in some sense the opposite of stress relaxation where the deformation of a material is observed under the influence of a constant rate of stress.

Viscoelasticity of soft tissues has been discussed under the realms of linear viscoelasticity and quantified by the use of models like the Maxwell, the Voigt and the Simple Linear Models [76]. This may be the case for small deformation of these materials. However, biomaterials developed of natural and synthetic polymers and some of the soft biological tissues display nonlinear viscoelastic behavior under the influence of large deformation. The most common and widely used model to characterize the nonlinear viscoelastic behavior is the Quasi Linear Viscoelastic (QLV) model, introduced by Fung [24] and later modified by many others according to comply with specific test or material requirements [25-31]. QLV theory assumes that the stress relaxation of soft tissues can be expressed as a product of a reduced relaxation function and the instantaneous stress

resulting from a ramp strain as:

$$\sigma(\varepsilon,t) = G(t)\sigma^e(\varepsilon(\tau)) \tag{1}$$

On applying the Boltzmann's superposition principle Eq.(1) can be expressed as,

$$\sigma(\varepsilon,t) = \int_{-\infty}^{t} G(t-\tau)\frac{\partial\sigma^e(\varepsilon(\tau))}{\partial\varepsilon}\frac{\partial\varepsilon(\tau)}{\partial\tau}d\tau \tag{2}$$

where $\frac{\partial\sigma^e(\varepsilon(\tau))}{\partial\varepsilon}$ represents the derivative of the instantaneous elastic response, $\frac{\partial\varepsilon(\tau)}{\partial\tau}$ is the strain history. In practical experiments, the applied strain history is considered to begin from time t=0. Hence, the lower limit in Eq.(2) is modified to

$$\sigma(\varepsilon,t) = \int_{0}^{t} G(t-\tau)\frac{\partial\sigma^e(\varepsilon(\tau))}{\partial\varepsilon}\frac{\partial\varepsilon(\tau)}{\partial\tau}d\tau \tag{3}$$

where $\sigma(\varepsilon,t)$ is the stress at any time t, $\sigma^e(\varepsilon(\tau))$ is the instantaneous elastic response (the maximum stress corresponding to an instantaneous step input of strain ε), G(t) is the reduced relaxation function that represents the time-dependent stress response of the tissue normalized by the stress at the time of the step input of strain. For soft tissues, Fung proposed a generalized reduced relaxation function equation based upon a continuous spectrum of relaxation which has the form

$$G(t) = \frac{1 + C[E_1(t/\tau_2) - E_1(t/\tau_1)]}{1 + C\ln(\tau_2/\tau_1)} \tag{4}$$

where *C* is a dimensionless material parameter that reflects the magnitude of viscous effects present, and is related to the fraction of relaxation. τ_1 and τ_2 are time-constants

that regulate the short and long-term material responses, relating to the slope of the stress-relaxation curve at early and late time periods, respectively. $E_1(t/\tau)$ is the exponential integral function of the form

$$E_1(t/\tau) = \int_{t/\tau}^{\infty} \frac{e^{-z}}{z} dz \tag{5}$$

If τ_1 and τ_2 differ sufficiently that $\tau_1 << t << \tau_2$, then Eq.(4) can be written [30] as

$$G(t) = \frac{1 - C\gamma - C\ln(t/\tau_2)}{1 + C\ln(\tau_2/\tau_1)} + \mathrm{O}(C) \tag{6}$$

where γ is the Euler constant which has a value of 0.5772 and O(C) is small and can be neglected. Thus

$$G(t-\tau) = \frac{1 - C\gamma - C\ln\left(\frac{t-\tau}{\tau_2}\right)}{1 + C\ln(\tau_2/\tau_1)} \tag{7}$$

Abramowitch and Woo in their modeling approach to quantify the viscoelastic behavior of the collateral ligament in a goat model [25], used the basic QLV modeling approach developed by Fung. They used the form of the reduced relaxation function shown in Eq.(4). The form of the instantaneous stress response used in their approach is given by an exponential approximation to the material nonlinear behavior as

$$\sigma^e(\varepsilon) = A\left(e^{B\varepsilon} - 1\right) \tag{8}$$

where A is the elastic stress constant with units of stress (MPa), and B is the dimensionless elastic power constant.

Finally, to generate the model equations the form of Eq.(4) and Eq.(8) are substituted in Eq.(1) to obtain

$$\sigma(t:0<t<t_0,\theta)=\frac{AB\gamma}{1+C\ln(\tau_2/\tau_1)}\int_0^t\{1+C(E_1[(t-\tau)/\tau_2]-E_1[(t-\tau)/\tau_1])\}e^{B\gamma\tau}\partial\tau \tag{9}$$

$$\sigma(t:t\geq t_0,\theta)=\frac{AB\gamma}{1+C\ln(\tau_2/\tau_1)}\int_0^{t_0}\{1+C(E_1[(t-\tau)/\tau_2]-E_1[(t-\tau)/\tau_1])\}e^{B\gamma\tau}\partial\tau \tag{10}$$

For the solution of Eqs.(9) and (10), Abramowitch and Woo made use of a modified Levenberg-Marquardt algorithm using the math solver Mathematica. The five model parameters, A, B, C, τ_1, and τ_2 were determined by the minimization of the Sum Squared Errors (SSE) between the experimental obtained data and theory as the objective function. This was performed simultaneously for the loading (Eq.(9)) and relaxation (Eq.(10)) equations. To ensure successful convergence the initial guess for each parameter was multiplied by a random factor between 0.1 and 10 and regression was performed 100 times with different initial guesses.

An alternative form of the stress relaxation function has also been used [29, 77], where the reduced relaxation function is of a different form than in Eq.(4) and is defined as

$$G(t)=ae^{-bt}+ce^{-dt}+ge^{-ht} \tag{11}$$

where a, b, c, d, g and h are parametric constants. The equation for the instantaneous stress function is of the same exponential form as Eq.(8).

For the form of reduced relaxation function used in Eq.(11) when the integral form of Eq.(3) is solved analytically, the output stress equations for the loading as well as the relaxation parts were obtained as shown [78]:

Loading Part: initial constant strain-rate conditions

$$\sigma(0 \le t \le t_0) = AB\gamma \left[\frac{a\left(e^{B\gamma t} - e^{bt}\right)}{b + B\gamma} + \frac{c\left(e^{B\gamma t} - e^{dt}\right)}{d + B\gamma} + \frac{g\left(e^{B\gamma t} - e^{ht}\right)}{h + B\gamma} \right] \qquad (12)$$

Relaxation Part: sample held at strain at end of loading period

$$\sigma(t > t_0) = AB\gamma \left[\frac{ae^{-bt}\left(e^{(b+B\gamma)t_0} - 1\right)}{b + B\gamma} + \frac{ce^{-dt}\left(e^{(d+B\gamma)t_0} - 1\right)}{d + B\gamma} + \frac{ge^{-ht}\left(e^{(h+B\gamma)t_0} - 1\right)}{h + B\gamma} \right] \qquad (13)$$

For the analytical form of Eqs.(12) and (13) the model parameters determined by least square approximation fail to display a physical significance to the material behavior under stress relaxation.

Different form of reduced relaxation function expressions have also been used to obtain the output stress. For example, Duling *et al.*, reported on viscoelastic stress relaxation characteristics of a scaffold made of PCL by the QLV model [23].the reduced relaxation function of the form of Eq.(7) was used to determine the material parameters. This form of the reduced relaxation function is also used in other reports [30].

.

CHAPTER III

COMPOSITE SCAFFOLD GENERATION

Combing synthetic and natural polymers is an approach to develop superior scaffolds for tissue engineering. Based on this concept, composite scaffolds have been formed. This chapter deals with the formation of the PLGA composite structure formed of a thin mechanically strong air dried film of PLGA sandwiched between porous structures of gelatin-chitosan by the process of controlled rate of freezing and freeze drying. .

3.1. Materials and Methods:

3.1.1. Materials: For the purpose of generating the PLGA composite scaffold the 50:50 PLGA polymer pellets, ester terminated (nominal) with 90-120 kDa Mw were obtained from LACTEL absorbable polymers (Pelham, AL), the chitosan (200-300 kDa molecular weight, Mw, 85% DD) and gelatin type – A (300 Bloom) were obtained from Sigma Aldrich Chemical (St. Louis, MO), Apper Ethyl Alcohol, 200 proof, anhydrous and chloroform were obtained from Pharmaco.

3.1.2. Method: The PLGA composite scaffolds were prepared by the method previously reported [10] with modifications. The steps for the process are explained briefly

- Step (1) involves forming a thin PLGA film by air drying PLGA solution (4 %

wt/v) prepared by dissolving the polymer pellets in 5mL chloroform, overnight in a chemical fume hood on a Teflon sheet (United States Plastic, Lima, OH) (8cm ×6cm) fixed to a flat aluminum plate **(Figure 2[1])**. The formed PLGA film as a result of air drying has a smooth and hydrophobic surface.

- Step (2) is the etching process where the formed PLGA film was completely submerged in 1N NaOH solution for 10 minutes **(Figure 2[2])**. This helps to create surface roughness on the smooth surface of PLGA film and also makes it hydrophilic.
- Step (3) involves washing the etched PLGA film with excess water and punching holes on the surface in a square pitch 1 cm apart from each other using a stainless steel needle and a hammer **(Figure 2[3])**.
- Finally, Step (4) involves layering the PLGA film with a 3 mL mixture of 0.5% (wt/v) chitosan and 0.5% (wt/v) gelatin solution dissolved in 0.7% (v/v) acetic acid, on both sides and freeze drying it in a lyophilizer to form the porous layer **(Figure 2[4])**.

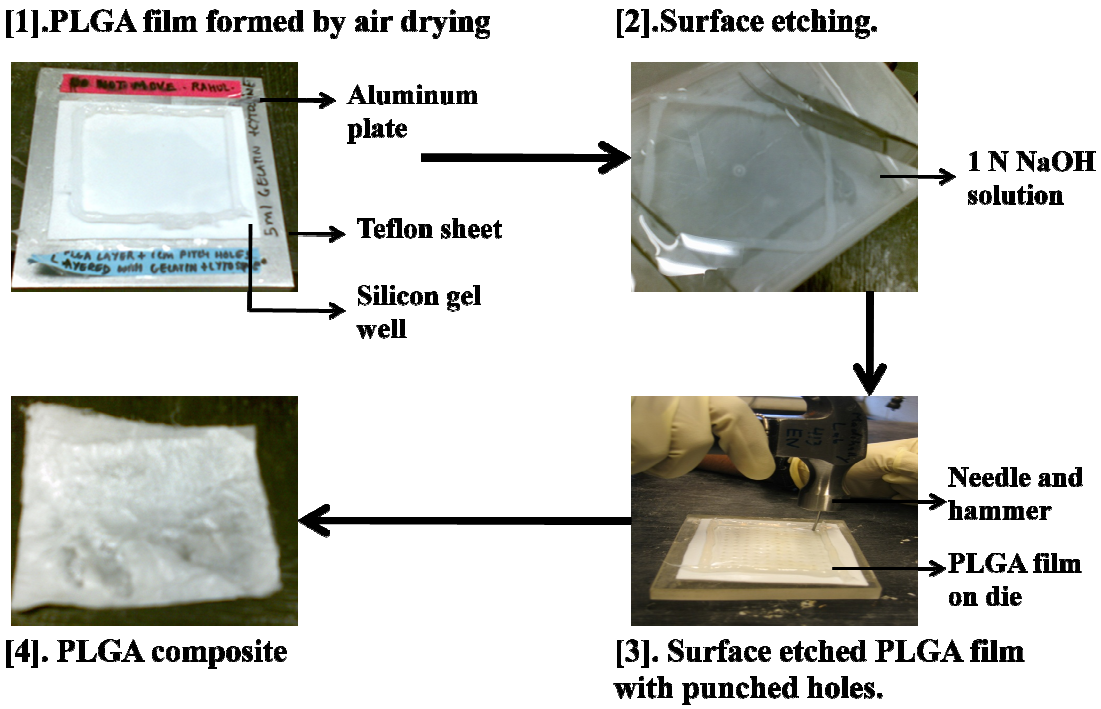

Figure 2: Steps to generate the PLGA composite scaffold with porous layer of gelatin-chitosan.

3.2. Surface Analysis of Etched PLGA using Scanning Electron Microscopy (SEM):

The effect of etching on the surface of the PLGA was analyzed via SEM. For this purpose, small, rectangular (2mm×3mm approx) pieces were cut out from both the untreated (unetched) and the 10 minute treated (etched) samples and were glued onto the surface of a metallic stud using either carbon dot or carbon paint. This was then splutter coated with gold-palladium in a splutter coater. The coated, dehydrated samples were then placed inside the SEM under conditions of vacuum. Pictures of the surface were taken at different accelerating voltages and different magnifications.

3.3. Results:

3.3.1. Effect of Etching Process on Surface Roughness of PLGA, SEM Analysis: The

SEM results showed **(Figures 3[A] and [B])** a difference in the surfaces between the unetched and 10 minute etched samples. The surface of the 10 minute etched sample displayed nanoscale surface features and other irregularities.

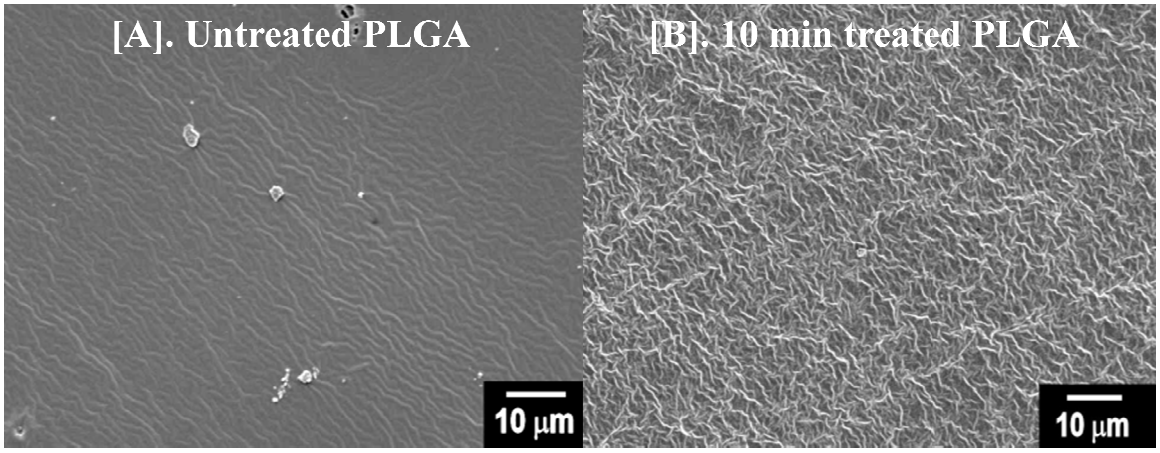

Figure 3: Scanning Electron Microscope (SEM) images of [A].the untreated, [B].the 10 min treated PLGA films.

3.3.2. Effect of Etching Process on the Mechanical Integrity of the Composite Scaffold: To understand the effect of etching the surface of the PLGA would have on the mechanical integrity of the composite structure the formed composite with and without the etching process was evaluated under SEM **(Figure 4[A] and [B])**. A very good contact between the non-porous PLGA membranes and the porous chitosan-gelatin region was observed **(Figure 4[B])** for the composite formed using the etching process. The composite formed without the etching process displayed separation of layers **(Figure 4[A])**. The dry thickness of these composite scaffolds was less than 1 mm and the PLGA membrane contributed less than 50 µm (~20 -30 µm). A reduction in thickness was achieved relative to composites formed without etching [10]. This reduction is attributed to the roughness created by the etching process which facilitated easy distribution of chitosan-gelatin solution. No separation of layers occurred when the samples were

neutralized with ethanol and hydrated in PBS.

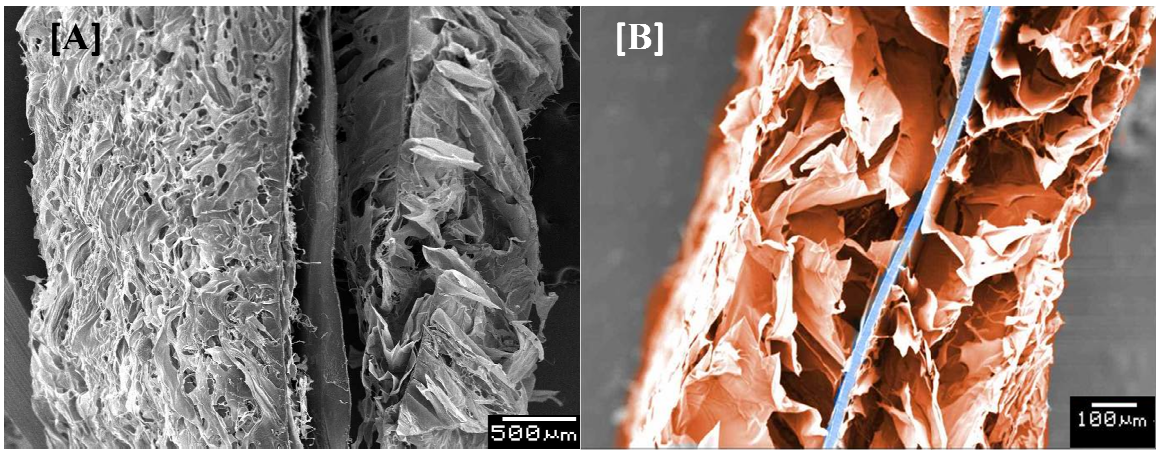

Figure 4: Cross sectional Scanning Electron Microscope (SEM) image of [A]. The PLGA composite formed without the etching process (Lawrence B.J.), [B] the PLGA composite formed using the etching process, shows good contact between the chitosan-gelatin porous structures to the PLGA layer.

SUMMARY: This work explored a novel method of generating composite scaffolds using the technique of etching which produces nanoscale surface features on the surface of a PLGA film. Porous compartment provides scaffolding for multilayered cell growth, while the membrane layer provides mechanical strength

The etching process increased the surface roughness of PLGA as observed from SEM analysis, similar to other published reports [79, 80], allowing easy spreading of natural polymers on its surface. The surface etching of PLGA also allowed better adherence of the chitosan-gelatin porous structure thereby maintaining the integrity of the composite structure.

CHAPTER IV

UNIAXIAL TENSILE ANALYSIS

Uniaxial tensile testing provides the break stress and strain values for the sample under consideration which acts as a gauge or provides a range of operation to conduct further mechanical analysis on the sample.

4.1. Thickness Measurement:

The thickness and the width of the sample are important for calculating the cross sectional area which in turn is necessary to calculate the resultant stress corresponding to strain generated during Uniaxial Tensile analysis. Thickness of the formed composite structures was measured by aligning wide strips of the composite orthogonally **(Figure 5[A])** to the plane of view of an inverted microscope [10, 81]. Thickness measurements were made using Sigma Scan Pro (SYSTAT Software, Point Richmond, CA) software at more than 40 locations **(Figure 5[B])** and average values were used in tensile testing. The system was calibrated using the image of a haemocytometer.

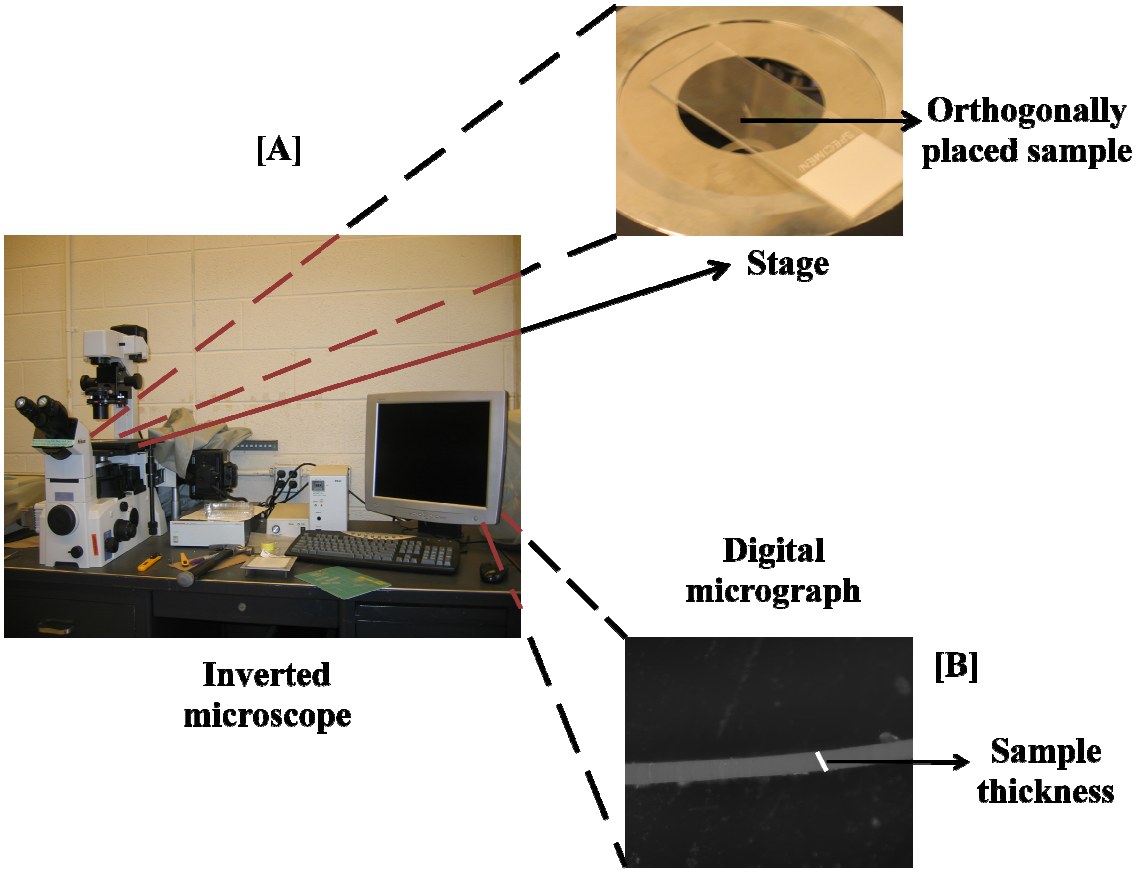

Figure 5: [A].Thickness measurement using an inverted microscope, [B].Image of the sample thickness as viewed from the microscope.

4.2. Uniaxial Tensile Testing:

For the tensile testing, 5cm×1cm strips were cut out from the sample specimen and strained to break at 10 mm/min crosshead speed using an INSTRON 5542 testing machine (INSTRON, Canton, MA) **(Figure 6[A] and [B])**. Testing was done under hydrated condition using Phosphate Buffered Saline (PBS) at 37°C using a chamber custom built in-house. Break stress and strain were determined using the associated software, Merlin (INSTRON Canton, MA). The output data for the engineering stress (MPa) is plotted against the engineering strain (%) using the software Sigma Plot

(SYSTAT Software, Point Richmond, CA).

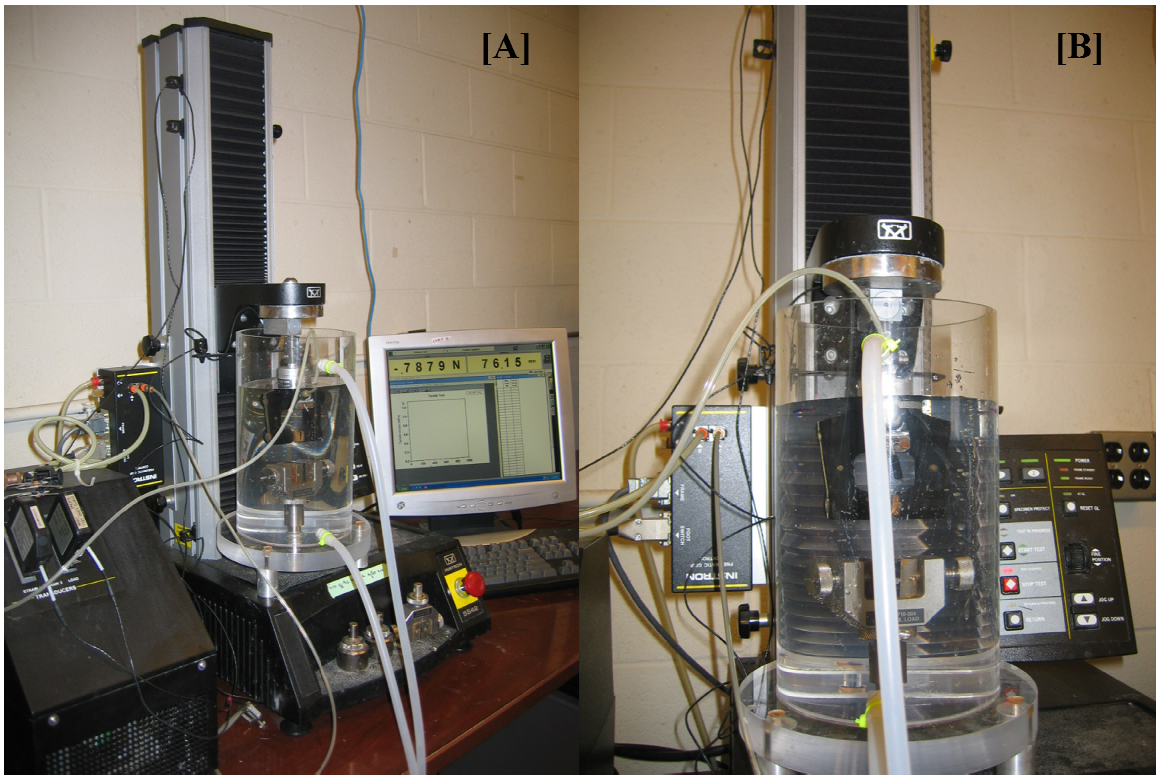

Figure 6: [A] INSTRON 5542 testing machine, [B] Special chamber built in-house to keep the sample hydrated during the testing

4.3. Results:

4.3.1. Uniaxial Tensile Testing of PLGA Composite: These results show **(Figure 7[A] and [B])** that the SIS and the composite have a similar range of break stress (~3-4 MPa). The break strain for the composite (~400%) is 6-8 times higher than that for SIS (~40-50%). The break strain value determines the input for the "Ramp-and-Hold" stress relaxation tests.

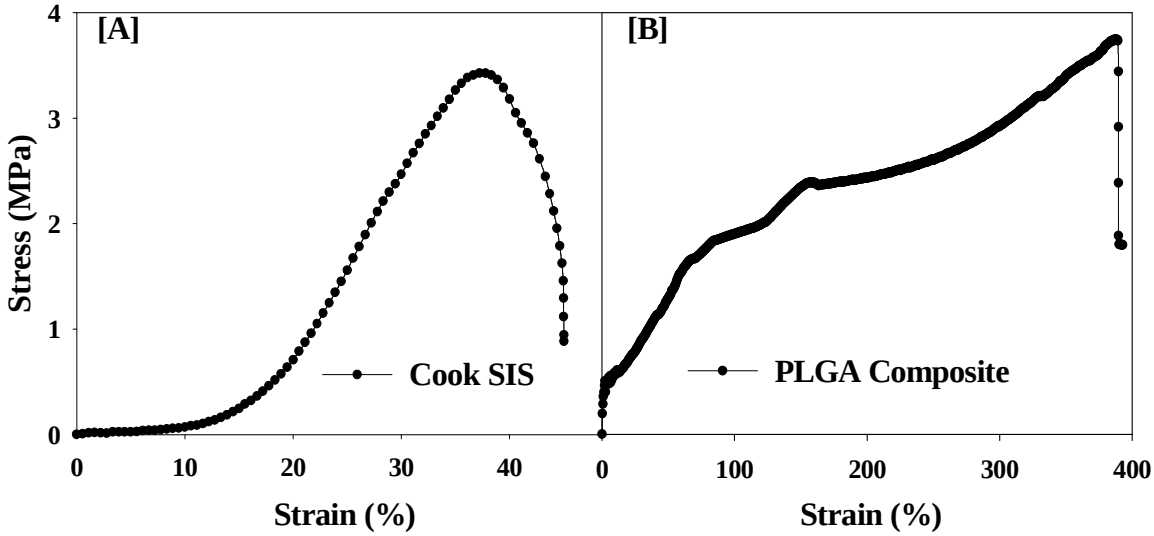

Figure 7: [A]. Stress vs. strain curve for the natural matrix SIS, [B]. Stress vs. strain curve for the PLGA composite.

4.3.2. Effect of Processing on Tensile Property of Composite: To assess the effect of processing, the unetched, the 10 minute etched, and the composite PLGA samples were tested under similar conditions. These results (**Figure 8**) showed that the composite failed at a strain value lesser than the unetched or the 10 minute etched sample. This suggested that the processing step of controlled rate of freezing and freezing drying affected the tensile strain of PLGA. Further, the chitosan-gelatin porous layer failed at around 200% of strain.

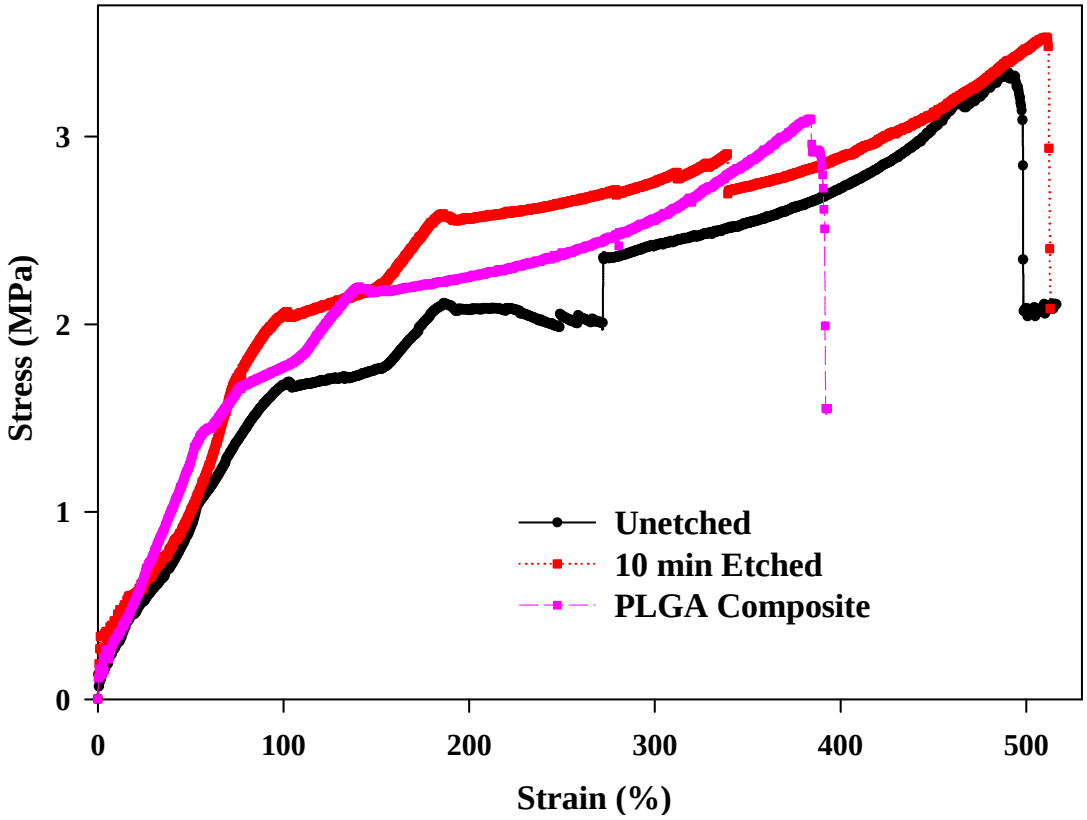

Figure 8: Stress vs. strain graph for the unetched, the etched, and the composite PLGA.

SUMMARY: Tensile testing analysis showed that ten minutes of this etching process did not affect the tensile properties of PLGA while providing sufficient roughness. This condition was used to form composite structures and the formed composites also displayed excellent tensile properties, the tensile strain at break being ~ 450%. This is nearly 6-8 times the break strain as that for SIS.

CHAPTER V

VISCOELASTIC STRESS RELAXATION ANALYSIS

The viscoelastic properties of the PLGA composite scaffold were assessed by performing "Ramp-and-Hold" type of stress relaxation experiments. Tensile analysis of the structure provided the range to operate without reaching the break strain. The "Ramp-and-Hold" test consists of two portions. The first portion is where a constant rate of tensile strain is applied to the sample for a predetermined amount of strain. This is called the ***loading portion***. The successive portion of the test is where the relaxation behavior of the specimen is observed under zero rate of loading by holding the sample at the strain value recorded at the end of the loading portion, is called the ***relaxation portion***.

5.1. Ramp and Hold Stress Relaxation Tests:

"Ramp-and-Hold" stress relaxation experiments were performed on the unetched, the etched, and the composite PLGA structures in succession of four ramps using the INSTRON 5542 universal testing machine. Each ramp had a loading part where the sample was loaded to 50% strain with a loading rate of 3.125 % s^{-1} and a 100 second relaxation part. The step-by-step procedure used to set up the stress relaxation test using the associated Merlin (INSTRON, Canton, MA) software is described in **Appendix 1**.

The relaxation time period of 100s was chosen because a previous study by Sauren, *et al*. showed that the majority of the relaxation in a material occurs in the first 100 seconds [82]. All experiments were conducted under physiological conditions, meaning at 37°C

and hydrated in PSB. Prior to testing the PLGA composite, samples were washed with ethanol to neutralize the excess acid encountered during the generation process. Stress and strain for the entire duration of the test were reported using Merlin. A stress vs. time graph was plotted to map the relaxation using the graphing software Sigma Plot (SYSTAT Software, Point Richmond, CA).

Relaxation for all the three samples was also compared by the means of a normalized stress function plot **(Figure 10)**. The normalization of the experimental stress at any time t during the relaxation part of the test is done by calculating the ratio of the stress at any time t, $\sigma(t)$ to the peak stress σ_p at time t_0. Mathematically it is represented as

$$G(t) = \frac{\sigma(t)}{\sigma_p} \tag{14}$$

All experiments were repeated three or more times with triplicate samples for each group and the data was reported in the graphical form as mean $\pm$ standard deviation values for all the samples at a regular interval of five seconds.

5.2. Variable Testing Conditions:

In order to understand the effect of variable loading rate, effect of temperature and also the effect of relaxation time on the stress relaxation behavior of PLGA, samples were tested under

a) Two different strain rates of 3.125 % s^{-1} and 12.5 % s^{-1}.
b) Two different values of relaxation times (60s and100s), and
c) Two different environmental temperatures (25°C and 37°C) in hydrated conditions.

5.3. Comparison of PLGA Composite to SIS:

Stress relaxation of PLGA composite was compared to SIS, both by the means of a stress vs. time plot and by calculating the percentage relaxation. For the SIS, tensile analysis reveal that the break strain ranges from 60-80% [81]. Hence, the amount of strain per ramp was reduced to 15% instead of the normal 50% as in the case of structures made out of PLGA. Further, in order to compare the relaxation properties of the PLGA composite, both SIS and the composite were subjected to a similar strain rate.

Percentage relaxation is a measure of the amount of relaxation that the material undergoes in successive cycles. It is calculated as the difference of the peak stress (σ_P) (stress at the end of the loading period) and the stress at the end of the relaxation period (σ_E) divided by the peak stress

$$\%relaxation = \left(\frac{\sigma_P - \sigma_E}{\sigma_P} \right) \times 100 \quad (15)$$

5.4. Results:

5.4.1. Ramp and Hold Stress Relaxation Test Results for the Unetched, Etched, and the Composite Structures Made of PLGA: The stress vs. time plot for the first ramp of the "Ramp-and-Hold" experiment on the unetched, the etched, and the composite PLGA structures is shown in **Figure 9.** As seen from the graph, the peak stress at the end of the loading period for the unetched PLGA sample (~1.8 MPa) is higher as compared to the etched and the composite PLGA samples (both ~ 0.8 – 0.9 MPa). This shows that the unetched sample accumulates more stress during loading than the etched and the composite structures.

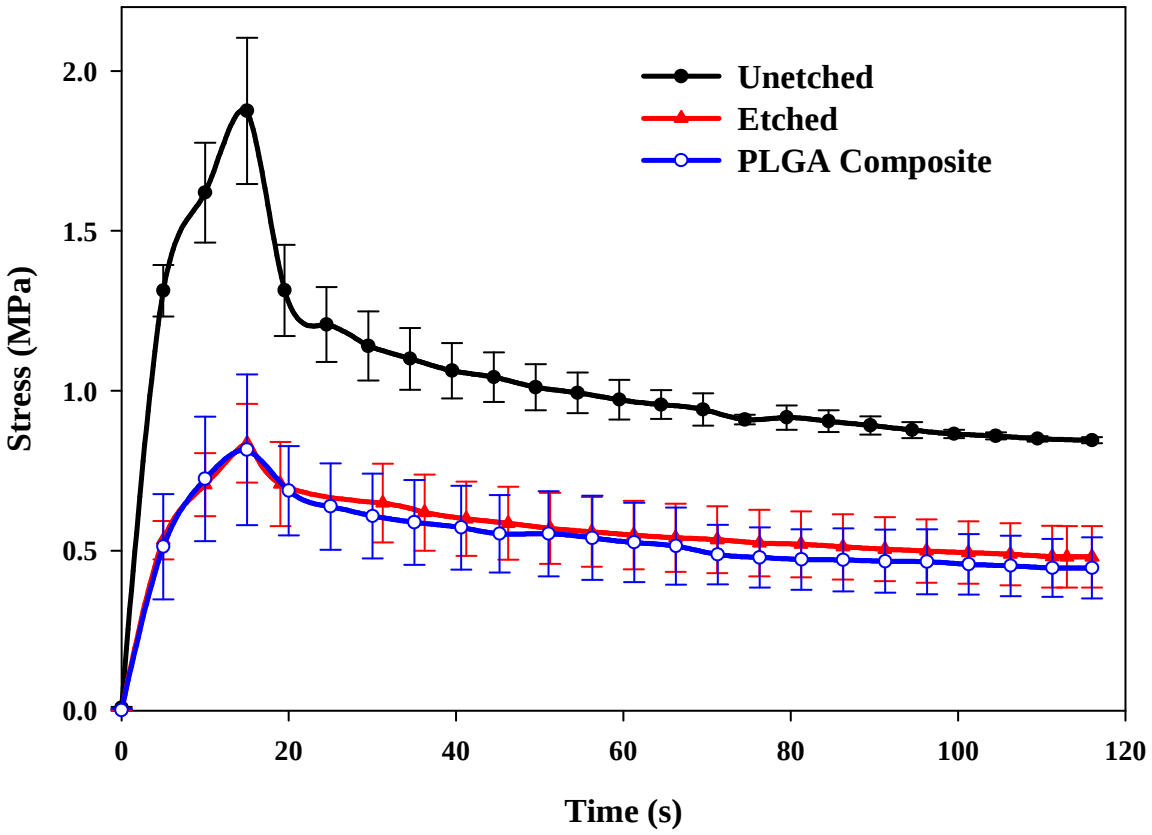

Figure 9: Stress vs. time plot of the unetched, etched, and composite samples as a result of "Ramp-and-Hold" stress relaxation tests.

5.4.2. Effect of Processing Steps on the Mechanical Characteristics of PLGA Composite: To understand the relaxation characteristics, stress values in the relaxation part of the first cycle was normalized with its peak stress. The plot of the normalized stress function (**Figure 10)** for the unetched PLGA sample is lower in magnitude than the etched and the composite PLGA samples. For the etched and the composite PLGA samples the reduced relaxation function plot is similar in magnitude. This indicates that the unetched sample relaxes better than the etched and the composite structures, which have similar relaxation values. Hence, it can be concluded that the etching process affects the relaxation properties of PLGA.

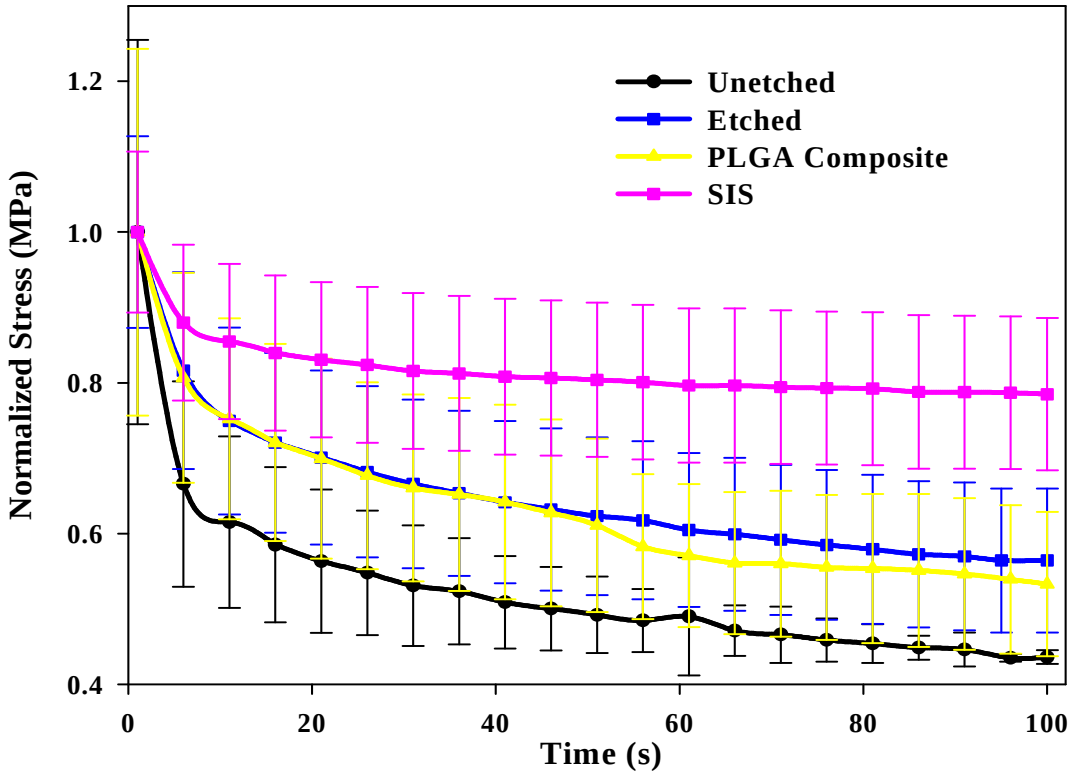

Figure 10: Normalized stress relaxation function plots for the unetched, etched, and composite PLGA.

5.4.3. Stress Relaxation of PLGA Structures Under Different Input Conditions: It was observed (**Figure 11**) that the trend of the stress vs. time plot under variable inputs remained the same. Under similar conditions of temperature and relaxation time (25°C and 100s) the magnitude of the peak stress at the end of loading for all the four ramps for the sample were found to be similar with changing the rate of loading from 3.125% s^{-1} to 12.5% s^{-1}. Upon changing the relaxation time from 60s to 100s **(Figure 11 [B])**, no major change in the peak stress was observed. However, changing the test temperature form 25°C to 37°C introduced a significant change in the peak stresses. Stresses were considerably lower at 37°C than at 25°C. This could be because at 37°C the material is much nearer its glass transition temperature (T_g, of PLGA~40-60 ° C). Polymers behave

as glassy materials near their T_g. Thus, the magnitude of peak stresses accumulated in PLGA structures after each loading cycle is affected more by the test temperature rather than the loading rate or the relaxation time.

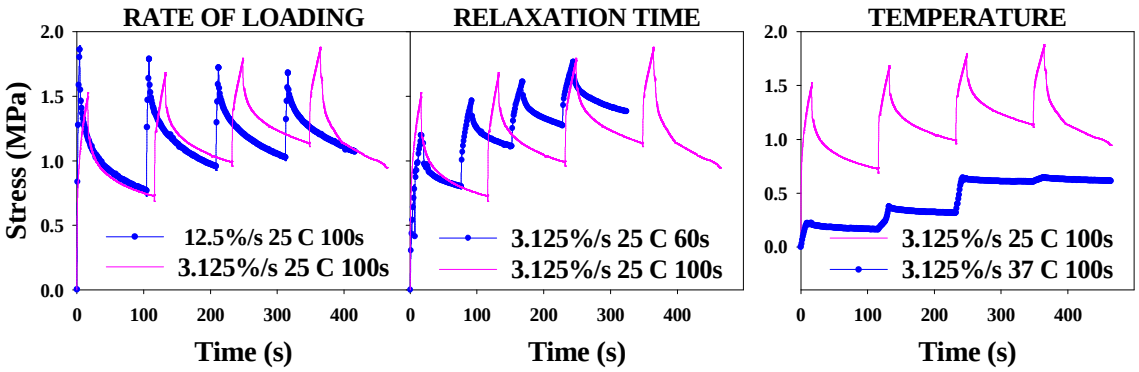

Figure 11: Stress relaxation of PLGA membranes; [A].Effect of loading rates ($3.125\%s^{-1}$ and $12.5\%s^{-1}$), [B].relaxation times (60 and 100s) and [C].different temperature values (25°C and 37°C).

5.4.4. Comparison to SIS: These results (**Figure 12**) show that, initially, for the first two ramps, the peak stress and the stress at the end of relaxation are lower for the SIS as compared to the composite structure. However, as the number of ramps increases, a reversal in the above mentioned trend is observed. For the SIS the peak stress in the first cycle was less than that developed in the fourth cycle. On the contrary, the peak stress developed in the first cycle for the composite was higher relative to the fourth cycle. This could mean that the composite has better relaxation behavior in the long run. Soft tissues are known to strain harden in successive cycles, and SIS also shows similar behavior. However, the composite behaved more like a strain softening material.

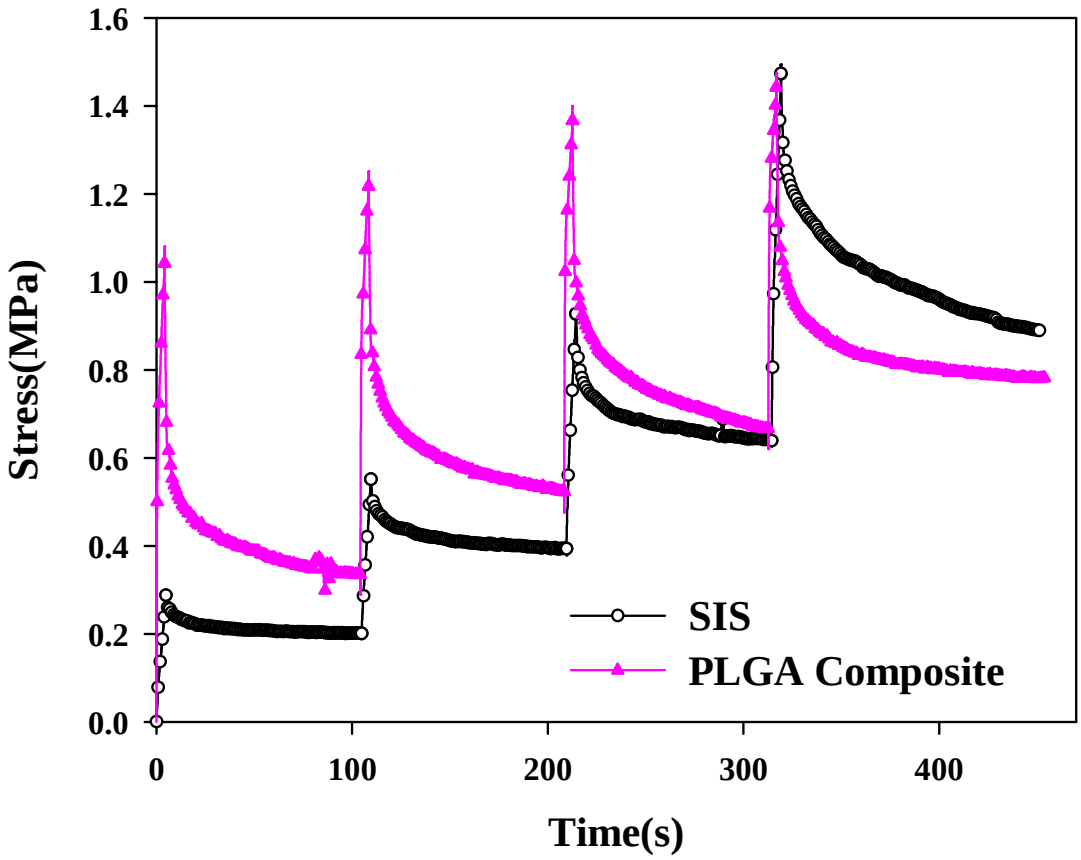

Figure 12: Comparison of the stress relaxation of the natural matrix SIS to the PLGA composite scaffold

SUMMARY: "Ramp-and-Hold" type stress relaxation experiments displayed higher stress accumulation for the unetched sample as compared to the etched and composite samples. Comparison of normalized stress function plots revealed better stress relaxation for the unetched sample. Also stress relaxation of all the structures made of PLGA is better than the SIS. This is in accordance to a study which say that the mechanical characteristics of polymeric structures is better than SIS [83]. Stress relaxation tests carried out at variable experimental conditions showed that the test temperature significantly affects the viscoelasticity of PLGA scaffolds. Consequently for variable loading rates and relaxation times peak stresses were found to be similar in magnitude.

This is in concurrence to the relaxation properties as observed for PCL by Duling *et al*, [23]. Interestingly, the plot for the ramping portion for the structures made of PLGA (concave downwards) was opposite to that of soft tissues (concave upwards) like ligaments, tendons, etc [23, 26, 29, 30, 84]. Also PLGA composite was found to be strain rate softening as compared to the strain rate hardening displayed by SIS.

CHAPTER VI

ANALYTICAL MODEL DEVELOPMENT, OPTIMIZATION, AND REGRESSION.

The analytical model used in this work to quantify the viscoelastic characteristic of PLGA based matrices is derived from the version of the QLV model as developed by Fung [85]. The model is formulated to eliminate the use of complex math solvers such as Mathematica, and Mat Lab. The optimization algorithm used to determine the model parameters is cyclic, heuristic and of a direct search class. It is developed by Dr. R Russell Rhinehart and the code is written in Visual Basic for Applications (VBA) with an interface in MS Excel. Regression is carried out by the simultaneous minimization of the SSE between the experimental data and model data as the objective function using the optimization algorithm.

6.1. Analytical Model Development:

The model is obtained by solving Eq.(3) analytically, after substituting the form of reduced relaxation function as in Eq.(7) and the form of the instantaneous stress response of Eq.(8). This procedure is done twice, separately for the loading and the relaxation parts with different limits. The limits for the loading part are 0 to t and that for the relaxation part being 0 to t_0. The final equation for the stress for the loading and the relaxation portion of the test are as follows

Loading part: initial constant strain-rate conditions

$$\sigma(0<t\le t_0)=\frac{A}{(1+C\ln(\tau_2/\tau_1)}\left[\left(e^{B\alpha t}-1\right)\left(1-C\gamma\right)+C\ln\left(\frac{t}{\tau_2}\right)-Ce^{B\alpha t}\ln(B\alpha t)+Ce^{B\alpha t}\sum_{k=1}^{\infty}\frac{(-1)^k(B\alpha t)^k}{kk!}\right] \tag{16}$$

Relaxation part: sample held at strain at end of loading period

$$\sigma(t\ge t_0)=\frac{A}{(1+C\ln(\tau_2/\tau_1)}\left[\left(e^{B\alpha t_0}-1\right)\left(1-C\gamma\right)+C\ln\left(\frac{t}{\tau_2}\right)-Ce^{B\alpha t_0}\ln\left(\frac{t-t_0}{\tau_2}\right)\right.$$
$$\left.-Ce^{B\alpha t}\ln\left(\frac{t-t_0}{\tau_2}\right)+Ce^{B\alpha t}\sum_{k=1}^{\infty}\frac{(-1)^k(B\alpha t)^k}{kk!}-Ce^{B\alpha t}\sum_{k=1}^{\infty}\frac{(-1)^k(B\alpha(t-t_0))^k}{kk!}\right] \tag{17}$$

Where α is the strain rate during loading. For complete derivation of Eqs.(16) and (17) refer to **Appendix 2.**

True stress and true strain values which account for the changes in cross section of the specimen [77, 86, 87] during the test are used for the nonlinear regression analysis to determine values for the constants A, B, C, τ_1 and τ_2 of the analytical model. True stress (σ_T) is approximated from the experimentally determined stress and strain (also referred as engineering stress and engineering strain) values using the equation

$$\sigma_T=\sigma_E\left(1+\varepsilon_E\right) \tag{18}$$

where σ_E is the engineering stress, and $\varepsilon_E$is the engineering strain. True strain (ε_T) [88, 89] is calculated using the equation

$$\varepsilon_T=\ln\left(1+\varepsilon_E\right) \tag{19}$$

where ε_E is the engineering strain.

6.2. Optimization Algorithm:

The optimization algorithm used in this work, the logic that directs the successive guess of the progressively improving model parameter values, is of the direct search class (only using objective function evaluation information), not of the gradient-based class (which uses first and second derivative information) and is developed by Dr. Russell R. Rhinehart. The optimization algorithm is a single-step, one variable at a time (cyclic) search with heuristic factors to either expand or contract-and-reverse subsequent steps depending on the past success of the step for that decision variable The cyclic, heuristic, direct search has advantages in simplicity and robustness. This direct search optimizer was coded in Visual Basic for Applications (VBA) with an interface in MS Excel. Refer **Appendix 3** for the algorithm

In order to avoid the dependence of the converged solution on the initial guess this algorithm incorporates the rule of "Best-of-N" and also a steady state stopping criterion to properly terminate the optimization.

6.2.1 "Best-of-N" Multi Start Criterion: This algorithm incorporates the "Best-of-N" method to determine the number of random starts in order to probably find the global minimum. The formula [32] to calculate this value of the number of starts, N, is

$$N = \frac{\ln(1 - P_{success})}{\ln(1 - \mathrm{f})} \tag{20}$$

where $P_{success}$ is the user-desired probability that the best from N independent optimizations will yield a SSE value which is one within the best fraction, f, of all

possible values. In this work, 22 iterations were used based on the desire to find out one of the best 10% of all possible objective function values at least once with 90% confidence.

$$N = \frac{\ln(1-0.90)}{\ln(1-0.10)} = 21.85 \tag{21}$$

To make the initial guesses different in every iteration, a randomization function available in VBA was used to generate random initial guesses for the decision variables from the defined parameter value range.

6.2.2. Stopping Criterion: The technique calculates the root-mean-squared (RMS) deviations from a randomly selected (RS) subset of the data at each iteration, and terminates optimization when the RMS-RS value shows no improvement with iteration number. This optimization termination has several advantages. It is scale-independent and single criterion, and does not require user-chosen thresholds. There are many ways to analyze for probable transient and probable steady state conditions. This method stops the iterations depending on a preset value of R, a ratio of variances, as measured on the same set of data by two different methods. At steady state the expected value of R is 1.

6.3. Objective Function:

Quantifying the viscoelastic stress relaxation behavior of the PLGA composite and also understanding the effect of the processing steps on the mechanical characteristics of the structure requires determining the phenomenological, parametric constants of the model (analytical model in this case) which have a physical significance. The objective function for the regression is the sum of squared errors (SSE) and the aim of the regression is to

minimize this SSE function. SSE is defined as the summation of square of the difference of the experimentally determined value to the analytically obtained value from the equation of stress. The SSE is calculated both for the loading as well as the relaxation part of the experimental data and can be represented mathematically as

$$SSE = \sum \left(\sigma_{\text{model data}} - \sigma_{\text{expermental data}} \right)^2 \tag{22}$$

6.4. Regression:

The analytically derived model equations (Eq.(16) and (17)) were simultaneously regressed by minimizing the sum squared errors (SSE) for the loading and relaxation parts as the objective function with the decision variables as the five model parameters, A, B, C, τ_1, τ_2. Unlike others [25, 29-31] which make use of the stress corresponding to instantaneous strain Eq.(8) to determine the values of A or B or A and B, this work regresses all five decision variables namely A, B, C, τ_1 and τ_2 together. Random initial guesses were generated for the model parameters by the optimizer for each of the N independent starts. Out of the N results obtained, the run with the minimum SSE value was chosen as the resulting value for the model parameters. The model equations are in the form of an infinite series and so the equations were truncated to the third order term as it was observed that the magnitude of the higher order terms was very small and insignificant compared to the function value.

Another approach which was tried in this work to obtain the analytical model parameters was doing the regression using the Newton's method in the Solver application in MS Excel. The strategy was similar to the above mentioned method, simultaneous

minimization of the SSE as the objective function. Parametric values generated using the Solver tool were found to be highly dependent on the initial guesses.

6.5. Results:

6.5.1. Result of Regression Analyses: The optimizer converged to several solutions for all the 22 random starts for a given sample (unetched, etched or composite). The trial with the minimum value of SSE obtained was selected with 90% confidence as belonging to one of the best possible 10% of all solutions (accepted as the global optimum). The comparisons of the curve fit of the experimental data to model are presented in **Figure 13** with parameter values presented in the form mean $\pm$ standard deviation of all data points for all the samples in **Table 1**. From **Table 1** it can be observed that the values of the model parameters governing the elastic behavior, A and B are higher for the unetched PLGA as compared to the etched and the composite PLGA. Accordingly the value of C, the model parameter that governs the viscous behavior is higher for the unetched sample indicating better relaxation.

6.5.2. Curve Fit Observation: Using parameters predicted from the analytical model, relaxation characteristics were predicted for different time points. Comparison of these results (**Figure 13)** revealed that the analytical model successfully predicts the experimental data for the SIS with less than 2% relative error. However, the model fails to obtain a good fit for the unetched, the etched and the composite PLGA samples. Nonetheless, it correctly predicts the trend observed in the relaxation portion of the experimental data for the three PLGA samples.

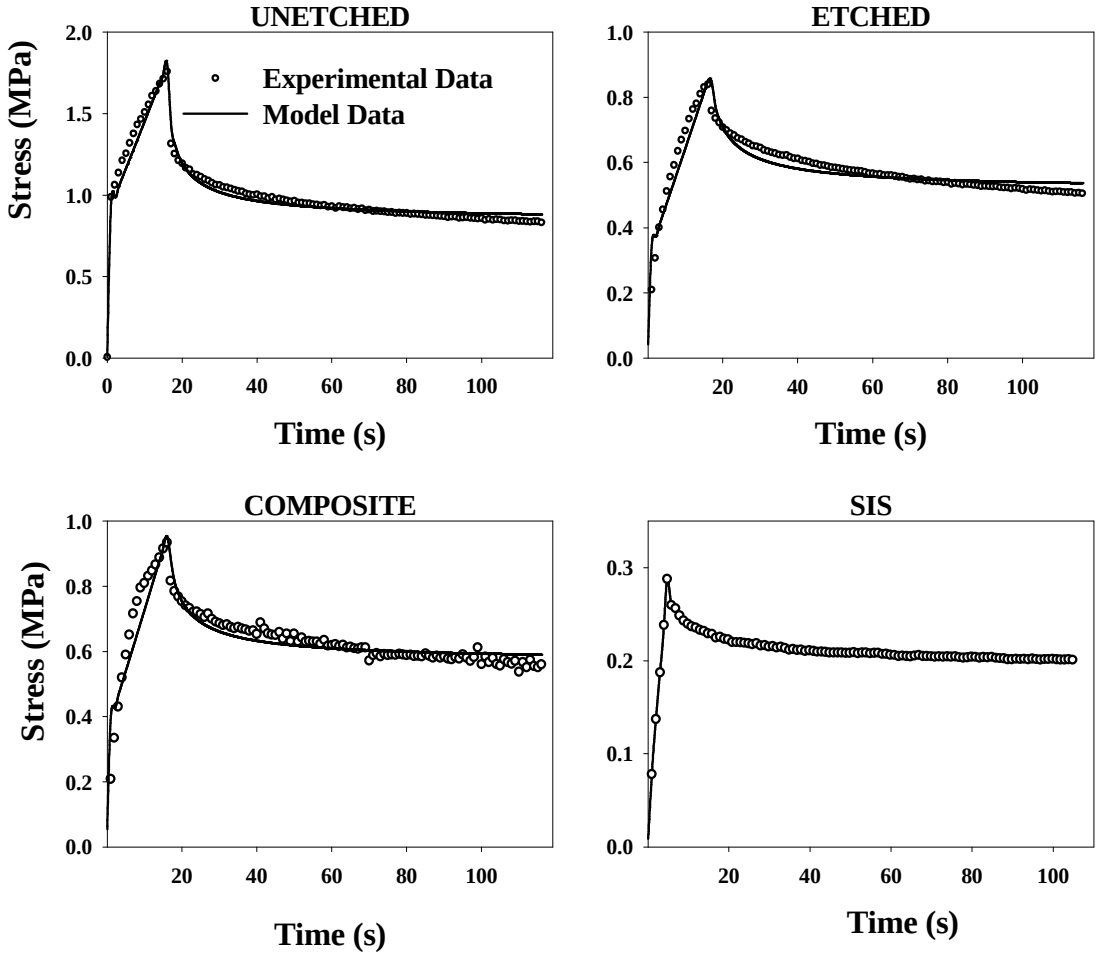

Figure 13: Curve fit: Regressed data and analytical model to the experimental data.

SAMPLE	A(MPa)	B	C	τ_1(s)	τ_2(s)
UNETCHED	13.92±1.11	0.1212±0.0051	0.008±0.002	0.18±0.2	412.7±199.5
ETCHED	10.35±0.45	0.104±0.004	0.006±0.00075	1.11±0.11	138.9±90.4
COMPOSITE	10.09±0.66	0.102±0.006	0.006±0.001	0.45±0.13	168.83±31.12
SIS	11.87±1.03	0.14±0.01	0.0024±0.0002	0.45±.92	90.5±8.1

Table 1: Parametric values for the analytical model determined using the optimizer

6.5.3. Comparison of Relaxation of PLGA Composite to SIS: The relaxation of the composite PLGA sample and the SIS were compared by the means of:

1. The normalized stress function plot: It can concluded from **Figure 10** that the normalized stress function plot for the PLGA composite is lower in magnitude than the SIS indicating that the composite relaxes better than the SIS with time.
2. The percentage relaxation values: Percentage relaxation is a measure of the amount of relaxation that the material undergoes as a result of a stress relaxation experiment. It is calculated as the difference of the peak stress at the end of the loading period and the stress at the end of the relaxation period divided by the peak stress. Mathematically it can be written as

$$\%relaxation = \left(\frac{\sigma_P - \sigma_E}{\sigma_P} \right) \times 100 \qquad (23)$$

The percentage relaxation values for the first ramp of the stress relaxation experiment for the composite is 67.86±1.81% as compared to 30.14±3.01% for SIS.

Sample Type	**% Stress Relaxation/Step (%)**			
	Step1	**Step2**	**Step3**	**Step4**
SIS	30.14±3.01	28.64±3.06	31.06±5.28	39.62±6.73
Composite	67.86±1.81	57.03±1.72	51.11±1.86	45.74±2.38

Table 2: Percentage stress relaxation values, per step, for the SIS and the composite.

SUMMARY: Higher value of parameter C indicated better stress relaxation of unetched PLGA compared to etched and composite PLGA indicating that etching affects the viscoelastic properties of PLGA. The analytical model successfully models the experimental data for SIS with less than 2% relative error. It, however, fails to correctly fit the experimental data for the structures made of PLGA.

CHAPTER VII

CONCLUSIONS AND RECOMMENDATIONS

The present study utilized a novel biomaterial scaffold made of a central layer of PLGA sandwiched between porous structures of chitosan-gelatin to characterize its viscoelastic properties by the application of the QLV model. This was done to understand its utility as a biomaterial to be used in tissue engineering applications. Conclusions from the study are summarized in accordance to the two specific aims

SPECIFIC AIM I: Evaluation of viscoelastic characteristics of porous scaffolds.

1. The etching process also affects the viscoelastic characteristics as accumulated peak stress during the loading phase of "Ramp-and-Hold" experiments for the unetched PLGA is twice as that of etched PLGA structures. The process of freezing and freeze-drying involved in the generation of composite PLGA scaffolds, however, has no effect on relaxation of PLGA structures. The etching process also reduces the overall thickness (nearly two folds) of the PLGA composite scaffold by allowing easy spreading of the chitosan-gelatin solution on its surface.

2. All the three PLGA structures (unetched, etched and composite) under the application of variable loading rates, relaxation times, and test temperatures display relaxation that is sensitive to change in the test temperature but not so to the change in the rates of loading

and relaxation times

3. Relaxation of the natural matrix SIS reveals that SIS, like the soft tissues in the body, displays strain rate hardening (higher peak stresses per step with increasing strain). In contrast, the PLGA composite scaffold displays strain rate softening (lower peak stresses per step with increasing strain).

SPECIFIC AIM II: Analysis of stress relaxation by Quasi Linear Viscoelastic model.

1. The QLV model was successfully applied with modifications to quantify the relaxation of PLGA structures for the first loading cycle. Output values of stress as evaluated from the model fits the experimental data with less than 5% relative error. All the five model parameters (A, B, C, τ_1, τ_2) generated using regression analysis are in the range of values reported in the literature for various soft tissues.

2. The QLV model parameter "C" reveals that stress relaxation of the unetched PLGA structure is better than that of the etched and composite PLGA structures. This is also reflected in the reduced relaxation function plot for the three structures. Relaxation values were lower in magnitude for the unetched PLGA as compared to the etched and the composite PLGA structures. This confirms that etching affects the relaxation viscoelastic properties of PLGA. The process of freezing and freeze-drying involved in the generation of composite PLGA scaffolds showed no effect on relaxation properties.

3. Comparison of the QLV model parameters for the SIS and the PLGA composite scaffold reveals that, PLGA composite scaffold relaxes better than SIS. This is

confirmed by the reduced relaxation function plots and percentage relaxation per step for the two structures.

RECOMMENDATIONS:

1. The stress relaxation of the PLGA structures was characterized by conducting uniaxial tensile as well as stress relaxation experiments. Native tissues in the body, depending on their location and function, are exposed to uniaxial as well as biaxial loading conditions. Biaxial stress relaxation experiments have been previously conducted to understand the stress relaxation of soft biological tissues [90]. Hence, for further analyses of stress relaxation, the composite structure could be tested under biaxial loading conditions.

2. The postulate that novel biomaterials should possess mechanical properties that mimic the native tissues is a good starting point in designing them. As previously understood, different tissue structures in the body are structurally and functionally different. This work explored a single biomaterial formed of PLGA with a comparison to the soft tissue structures in the body. Thus the premise that novel biomaterials must mimic native tissue mechanical characteristics leaves room for a whole gamut of material and mechanistic models to be tested.

3. There are several fundamental problems in the acceptance and application of the QLV model, which are listed in literature [91], and experienced here. With respect to its derivation, the redundancy in the A and B coefficients are visible in the analytical expressions of Eqs.(16) and (17), assumptions in the constitutive relations of Eqs.(4) to (7) are not defended, and the nonlinearity of Eq.(8) violates Boltzmann's superposition

conditions of the convolution integral. With respect to its application, the redundancy in the QLV model is often accounted for by fixing either the value of coefficient A or B, and then optimizing the other parameters. But, this is not necessarily a correct approach to undesirable model functionality. If the product Bε becomes very small then the nonlinear Eq.(8) becomes a linear equation, making A and B redundant coefficients. This supports the choice of a linear instantaneous stress model to predict this behavior. Further, if data from the ramp strain is used to determine values for Eq.(8) coefficients, this implicitly assumes that there is no relaxation during the ramp strain. G(t) used is obtained by truncation of an infinite series. This might cause errors in estimating the values of the decision variables. Hence, there is need for a robust, phenomenological model based purely on the material behavior devoid of assumptions and an optimization strategy to predict the constants of this model with the highest accuracy. The QLV model was formulated predominantly for predicting the strain and time dependent viscoelastic characteristics of soft tissues. It assumes the application of a step strain followed immediately by relaxation. It also assumes that the stress developed as a result of the step of strain can be separated into a time dependent relaxation and a stretch dependent loading function. Practically, however, it is impossible to realize an instantaneous step of load and so researchers apply ramp loading at a very fast rate for a finite amount of time. As a result of the instantaneous step loading some relaxation occurs during the loading phase which remains unaccounted. This introduces in the determination of the relaxation constants of the QLV model, especially τ_1. These errors can be minimized by using the full constitutive form of Eq.(3) as it is done in this work [25, 92-94].

REFERENCES:

1. Chvapil M. Collagen sponge: theory and practice of medical applications. Journal of Biomedical Materials Research 1977;11(5):721-741.

2. Oberpenning F, Meng J, Yoo JJ, Atala A. De novo reconstitution of a functional mammalian urinary bladder by tissue engineering. Nat Biotechnol 1999;17(2):149-155.

3. Raghavan D, Kropp BP, Lin HK, Zhang Y, Cowan R, Madihally SV. Physical characteristics of small intestinal submucosa scaffolds are location-dependent. J Biomed Mater Res A 2005;73A(1):90-96.

4. Tillman J, Ullm A, Madihally SV. Three-dimensional cell colonization in a sulfate rich environment. Biomaterials 2006;27(32):5618-5626.

5. Langer R, Tirrell DA. Designing materials for biology and medicine. Nature 2004;428(6982):487-492.

6. Moshfeghian A, Tillman J, Madihally SV. Characterization of emulsified chitosan-PLGA matrices formed using controlled-rate freezing and lyophilization technique. J Biomed Mater Res A 2006;79(2):418-430.

7. Sarasam A, Madihally SV. Characterization of chitosan-polycaprolactone blends for tissue engineering applications. Biomaterials 2005;26(27):5500-5508.

8. Mi FL, Lin YM, Wu YB, Shyu SS, Tsai YH. Chitin/PLGA blend microspheres as a biodegradable drug-delivery system: phase-separation, degradation and release behavior. Biomaterials 2002;23(15):3257-3267.

9. Wang YC, Lin MC, Wang da M, Hsieh HJ. Fabrication of a novel porous PGA-chitosan hybrid matrix for tissue engineering. Biomaterials 2003;24(6):1047-1057.

10. Lawrence BJ, Maase EL, Lin HK, Madihally SV. Multilayer composite scaffolds with mechanical properties similar to small intestinal submucosa. J Biomed Mater Res Part A 2009;88(3):634-643.

11. Jamison CE, Marangoni RD, Glaser AA. Viscoelastic properties of soft tissue by discrete model characterization. J Biomech 1968;1(1):33-46.

12. Lanir Y. Constitutive equations for fibrous connective tissues. J Biomech 1983;16(1):1-12.

13. Grashow JS, Yoganathan AP, Sacks MS. Biaixal stress-stretch behavior of the mitral valve anterior leaflet at physiologic strain rates. Ann Biomed Eng 2006;34(2):315-325.

14. Holzapfel GA, Eberlein R, Wriggers P, Weizsäcker HW. Large strain analysis of soft biological membranes: Formulation and finite element analysis. Computer Methods in Applied Mechanics and Engineering 1996;132(1-2):45-61.

15. Jacob X, Catheline S, Gennisson JL, Barriere C, Royer D, Fink M. Nonlinear shear wave interaction in soft solids. J Acoust Soc Am 2007;122(4):1917-1926.

16. Weiss JA, Gardiner JC, Bonifasi-Lista C. Ligament material behavior is nonlinear, viscoelastic and rate-independent under shear loading. J Biomech 2002;35(7):943-950.

17. Haslach HW, Jr. Nonlinear viscoelastic, thermodynamically consistent, models for biological soft tissue. Biomech Model Mechanobiol 2005;3(3):172-189.

18. Fung YC. Biomechanics. Mechanical Properties of Living Tissues 1982.

19. Olberding JE, Francis Suh JK. A dual optimization method for the material parameter identification of a biphasic poroviscoelastic hydrogel: Potential application to hypercompliant soft tissues. J Biomech 2006;39(13):2468-2475.

20. Doehring T, Einstein D, Freed A, Pindera M-J, Saleeb A, Vesely I. New approaches to computational modeling of the cardiac valves. 2004; Anaheim, CA, United States: Acta Press; 2004.134-137.

21. Picton DC, Wills DJ. Viscoelastic properties of the periodontal ligament and mucous membrane. J Prosthet Dent 1978;40(3):263-272.

22. Egorov V, Tsyuryupa S, Kanilo S, Kogit M, Sarvazyan A. Soft tissue elastometer. Medical Engineering & Physics 2008;30(2):206-212.

23. Duling RR, Dupaix RB, Katsube N, Lannutti J. Mechanical characterization of electrospun polycaprolactone (PCL): a potential scaffold for tissue engineering. J Biomech Eng 2008;130(1):011006.

24. Fung YC. Elasticity of soft tissues in simple elongation. Am J Physiol 1967;213(6):1532-1544.

25. Abramowitch SD, Woo SL. An improved method to analyze the stress relaxation of ligaments following a finite ramp time based on the quasi-linear viscoelastic theory. J Biomech Eng 2004;126(1):92-97.

26. Abramowitch SD, Woo SL, Clineff TD, Debski RE. An evaluation of the quasi-linear viscoelastic properties of the healing medial collateral ligament in a goat model. Ann Biomed Eng 2004;32(3):329-335.

27. Defrate LE, Li G. The prediction of stress-relaxation of ligaments and tendons using the quasi-linear viscoelastic model. Biomech Model Mechanobiol 2007;6(4):245-251.

28. Funk JR, Hall GW, Crandall JR, Pilkey WD. Linear and quasi-linear viscoelastic characterization of ankle ligaments. J Biomech Eng 2000;122(1):15-22.

29. Toms SR, Dakin GJ, Lemons JE, Eberhardt AW. Quasi-linear viscoelastic behavior of the human periodontal ligament. J Biomech 2002;35(10):1411-1415.

30. Woo SL, Gomez MA, Akeson WH. The time and history-dependent viscoelastic properties of the canine medical collateral ligament. J Biomech Eng 1981;103(4):293-298.

31. Woo SL, Peterson RH, Ohland KJ, Sites TJ, Danto MI. The effects of strain rate on the properties of the medial collateral ligament in skeletally immature and mature rabbits: a biomechanical and histological study. J Orthop Res 1990;8(5):712-721.

32. Iyer MS, Rhinehart RR. A method to determine the required number of neural-network training repetitions. IEEE Trans Neural Netw 1999;10(2):427-432.

33. Iyer MS, Russell Rhinehart R. Novel method to stop neural network training. 2000; Chicago, IL, USA: IEEE; 2000. 929-933.

34. Langer R, Vacanti JP. Tissue engineering. Science 1993;260(5110):920-926.

35. Vacanti CA. History of tissue engineering and a glimpse into its future. Tissue Eng 2006;12(5):1137-1142.

36. United Network Organ Sharing Statistics. 2009 http://www.unos.org/Resources/bioethics

37. Griffith LG, Naughton G. Tissue engineering current challenges and expanding opportunities. Science 2002;295(5557):1009-1014.

38. Tissues and Organs. Home Edition ed. NJ: The Merck Manuals, 2006.

39. Scott JH. Scaffold Design and Manufacturing: From Concept to Clinic. Advanced Materials 2009;21(32-33):3330-3342.

40. Rajan K. Linear elastic properties of trabecular bone: a cellular solid approach. Journal of Materials Science Letters 1985;4(5):609-611.

41. Harrison NM, McDonnell PF, O'Mahoney DC, Kennedy OD, O'Brien FJ, McHugh PE. Heterogeneous linear elastic trabecular bone modelling using micro-CT attenuation data and experimentally measured heterogeneous tissue properties. Journal of Biomechanics 2008;41(11):2589-2596.

42. Wilson W, van Donkelaar CC, van Rietbergen B, Ito K, Huiskes R. Stresses in the local collagen network of articular cartilage: a poroviscoelastic fibril-reinforced finite element study. Journal of Biomechanics 2004;37(3):357-366.

43. Suh J-K, Bai S. Finite Element Formulation of Biphasic Poroviscoelastic Model for Articular Cartilage. Journal of Biomechanical Engineering 1998;120(2):195-201.

44. Mak AF. The Apparent Viscoelastic Behavior of Articular Cartilage The Contributions From the Intrinsic Matrix Viscoelasticity and Interstitial Fluid Flows. Journal of Biomechanical Engineering 1986;108(2):123-130.

45. Huang C-Y, Mow VC, Ateshian GA. The Role of Flow-Independent Viscoelasticity in the Biphasic Tensile and Compressive Responses of Articular Cartilage. Journal of Biomechanical Engineering 2001;123(5):410-417.

46. García JJ, Cortés DH. A nonlinear biphasic viscohyperelastic model for articular cartilage. Journal of Biomechanics 2006;39(16):2991-2998.

47. Thomas GC, Asanbaeva A, Vena P, Sah RL, Klisch SM. A Nonlinear Constituent Based Viscoelastic Model for Articular Cartilage and Analysis of Tissue Remodeling Due to Altered Glycosaminoglycan-Collagen Interactions. Journal of Biomechanical Engineering 2009;131(10):101002-101011.

48. Oelschlager BK, Pellegrini CA, Hunter J, Soper N, Brunt M, Sheppard B. Biologic prosthesis reduces recurrence after laparoscopic paraesophageal hernia repair: a multicenter, prospective, randomized trial. Ann Surg 2006;244(4):481-490.

49. Petter-Puchner AH, Fortelny RH, Mittermayr R, Walder N, Ohlinger W, Redl H. Adverse effects of porcine small intestine submucosa implants in experimental ventral hernia repair. Surg Endosc 2006;20(6):942-946.

50. Mostow EN, Haraway GD, Dalsing M, Hodde JP, King D. Effectiveness of an extracellular matrix graft (OASIS Wound Matrix) in the treatment of chronic leg ulcers: a randomized clinical trial. J Vasc Surg 2005;41(5):837-843.

51. Ayyildiz A, Akgul KT, Huri E, Nuhoglu B, Kilicoglu B, Ustun H Use of porcine small intestinal submucosa in bladder augmentation in rabbit: long-term histological outcome. ANZ J Surg 2008;78(1-2):82-86.

52. Chen G, Sato T, Ushida T, Ochiai N, Tateishi T. Tissue engineering of cartilage using a hybrid scaffold of synthetic polymer and collagen. Tissue Eng 2004;10(3-4):323-330.

53. Lelkes PI, Li M, Perets A, Mondrinos MJ, Guo Y, Chen X, et al. Designing Intelligent Polymeric Scaffolds for Tissue Engineering: Blending and Co-Electrospinning

Synthetic and Natural Polymers. Experimental Analysis of Nano and Engineering Materials and Structures, 2007.831-832.

54. Chun-Jen L, Chin-Fu C, Jui-Hsiang C, Shu-Fung C, Yu-Ju L, Ken-Yuan C. Fabrication of porous biodegradable polymer scaffolds using a solvent merging/particulate leaching method. Journal of Biomedical Materials Research 2002;59(4):676-681.

55. Wu L, Jing D, Ding J. A "room-temperature" injection molding/particulate leaching approach for fabrication of biodegradable three-dimensional porous scaffolds. Biomaterials 2006;27(2):185-191.

56. Harris LD, Kim BS, Mooney DJ. Open pore biodegradable matrices formed with gas foaming. J Biomed Mater Res 1998;42(3):396-402.

57. Lam CXF, Mo XM, Teoh SH, Hutmacher DW. Scaffold development using 3D printing with a starch-based polymer. Materials Science and Engineering: C 2002;20(1-2):49-56.

58. Liu CZ, Xia ZD, Han ZW, Hulley PA, Triffitt JT, Czernuszka JT. Novel 3D collagen scaffolds fabricated by indirect printing technique for tissue engineering. Journal of Biomedical Materials Research Part B: Applied Biomaterials 2008;85B(2):519-528.

59. Chong EJ, Phan TT, Lim IJ, Zhang YZ, Bay BH, Ramakrishna S, et al. Evaluation of electrospun PCL/gelatin nanofibrous scaffold for wound healing and layered dermal reconstitution. Acta Biomaterialia 2007;3(3):321-330.

60. Mao JS, Zhao LG, Yin YJ, Yao KD. Structure and properties of bilayer chitosan-gelatin scaffolds. Biomaterials 2003;24:1067-1074.

61. http://en.wikipedia.org/wiki/Tissue_engineering

62. Madihally SV, Matthew HWT. Porous chitosan scaffolds for tissue engineering. Biomaterials 1999;20(12):1133-1142.

63. Huang Y, Onyeri S, Siewe M, Moshfeghian A, Madihally SV. In vitro characterization of chitosan-gelatin scaffolds for tissue engineering. Biomaterials 2005;26(36):7616-7627.

64. Mao J, Zhao L, De Yao K, Shang Q, Yang G, Cao Y. Study of novel chitosan-gelatin artificial skin in vitro. J Biomed Mater Res A 2003;64(2):301-308.

65. Xia W, Liu W, Cui L, Liu Y, Zhong W, Liu D, et al. Tissue engineering of cartilage with the use of chitosan-gelatin complex scaffolds. J Biomed Mater Res B Appl Biomater 2004;71(2):373-380.

66. Lawrence BJ, Madihally SV. Cell Colonization in Degradable 3D Porous Matrices. Cell Adhesion and Migration 2008;2(1):1-8.

67. Rajnicek A, Britland S, McCaig C. Contact guidance of CNS neurites on grooved quartz: influence of groove dimensions, neuronal age and cell type. J Cell Sci 1997;110(Pt 23):2905-2913.

68. Curtis A, Wilkinson C. New depths in cell behaviour: reactions of cells to nanotopography. Biochem Soc Symp 1999;65:15-26.

69. Salem AK, Stevens R, Pearson RG, Davies MC, Tendler SJ, Roberts CJ. Interactions of 3T3 fibroblasts and endothelial cells with defined pore features. J Biomed Mater Res 2002;61(2):212-217.

70. Zaleskas JM, Kinner B, Freyman TM, Yannas IV, Gibson LJ, Spector M. Growth factor regulation of smooth muscle actin expression and contraction of human articular

chondrocytes and meniscal cells in a collagen-GAG matrix. Exp Cell Res 2001;270(1):21-31.

71. Lee CR, Grodzinsky AJ, Spector M. The effects of cross-linking of collagen-glycosaminoglycan scaffolds on compressive stiffness, chondrocyte-mediated contraction, proliferation and biosynthesis. Biomaterials 2001;22(23):3145-3154.

72. Sieminski AL, Hebbel RP, Gooch KJ. The relative magnitudes of endothelial force generation and matrix stiffness modulate capillary morphogenesis in vitro. Exp Cell Res 2004;297(2):574-584.

73. Instron. Tensile Testing. http://www.instron.us/wa/applications/test_types/tension/default.aspx

74. Instron. Compression Test. Materials Testing Solutions http://www.instron.us/wa/applications/test_types/compression

75. Mirani RD, Pratt J, Iyer P, Madihally SV. The stress relaxation characteristics of composite matrices etched to produce nanoscale surface features. Biomaterials 2009;30(5):703-710.

76. Yang X, Church CC. A simple viscoelastic model for soft tissues in the frequency range 6-20 MHz. IEEE Trans Ultrason Ferroelectr Freq Control 2006;53(8):1404-1411.

77. Wills DJ, Picton DC, Davies WI. An investigation of the viscoelastic properties of the periodontium in monkeys. J Periodontal Res 1972;7(1):42-51.

78. Hollister SJ. Biosolid Mechanics: Modeling and Applications. Fitting Quasilinear Viscoelastic Constitutive Model Constants http://www.engin.umich.edu/class/bme456/ch8fitqlvconstant/bme456qlvfitmodel.htm

79. Park GE, Pattison MA, Park K, Webster TJ. Accelerated chondrocyte functions on NaOH-treated PLGA scaffolds. Biomaterials 2005;26(16):3075-3082.

80. Miller DC, Thapa A, Haberstroh KM, Webster TJ. Endothelial and vascular smooth muscle cell function on poly(lactic-co-glycolic acid) with nano-structured surface features. Biomaterials 2004;25(1):53-61.

81. Raghavan D, Kropp BP, Lin HK, Zhang Y, Cowan R, Madihally SV. Physical characteristics of small intestinal submucosa scaffolds are location-dependent. J Biomed Mater Res A 2005;73(1):90-96.

82. Sauren AA, van Hout MC, van Steenhoven AA, Veldpaus FE, Janssen JD. The mechanical properties of porcine aortic valve tissues. J Biomech 1983;16(5):327-337.

83. Arnold GA, Mathews KG, Roe S, Mente P, Seaboch T. Biomechanical comparison of four soft tissue replacement materials: an in vitro evaluation of single and multilaminate porcine small intestinal submucosa, canine fascia lata, and polypropylene mesh. Vet Surg 2009;38(7):834-844.

84. Nekouzadeh A, Pryse KM, Elson EL, Genin GM. A simplified approach to quasi-linear viscoelastic modeling. J Biomech 2007;40(14):3070-3078.

85. Fung Y-c. Biomechanics: Mechanical Properties of Living Tissues. 2 ed: Springer, 1993.

86. Craiem D, Rojo FJ, Atienza JM, Armentano RL, Guinea GV. Fractional-order viscoelasticity applied to describe uniaxial stress relaxation of human arteries. Phys Med Biol 2008;53(17):4543-4554.

87. Nagasawa S, Hayano K, Niino T, Yamakura K, Yoshida T, Mizoguchi T. Nonlinear stress analysis of titanium implants by finite element method. Dent Mater J 2008;27(4):633-639.

88. Shodor. True Stress and True Strain. http://www.shodor.org/~jingersoll/weave/tutorial/node3.html

89. Corporation DT. Engineering Strain Vs. True Strain. http://www.drd.com/searchable/techsupport/eng_true_strain.htm

90. Nagatomi J, Gloeckner DC, Chancellor MB, DeGroat WC, Sacks MS. Changes in the biaxial viscoelastic response of the urinary bladder following spinal cord injury. Ann Biomed Eng 2004;32(10):1409-1419.

91. Provenzano P, Lakes R, Keenan T, Vanderby R, Jr. Nonlinear ligament viscoelasticity. Ann Biomed Eng 2001;29(10):908-914.

92. Carew EO, Talman EA, Boughner DR, Vesely I. Quasi-Linear Viscoelastic Theory Applied to Internal Shearing of Porcine Aortic Valve Leaflets. Journal of Biomechanical Engineering 1999;121(4):386-392.

93. Kwan MK, Lin TH, Woo SL. On the viscoelastic properties of the anteromedial bundle of the anterior cruciate ligament. J Biomech 1993;26(4-5):447-452.

94. Miller CE, Vanni MA, Keller BB. Characterization of passive embryonic myocardium by quasi-linear viscoelasticity theory. J Biomech 1997;30(9):985-988.

95. Jan J. Tuma. Engineering mathematics handbook. 4 ed: McGraw-Hill Professional, 1998.

APPENDIX 1

STRESS RELAXATION TEST SETUP

Step 1:

- Start the INSTRON 5542 machine using the on/off switch at the back end of the machine.
- Open the MERLIN software by double clicking the MERLIN icon placed on the desktop.
- The window shown below appears on the screen.

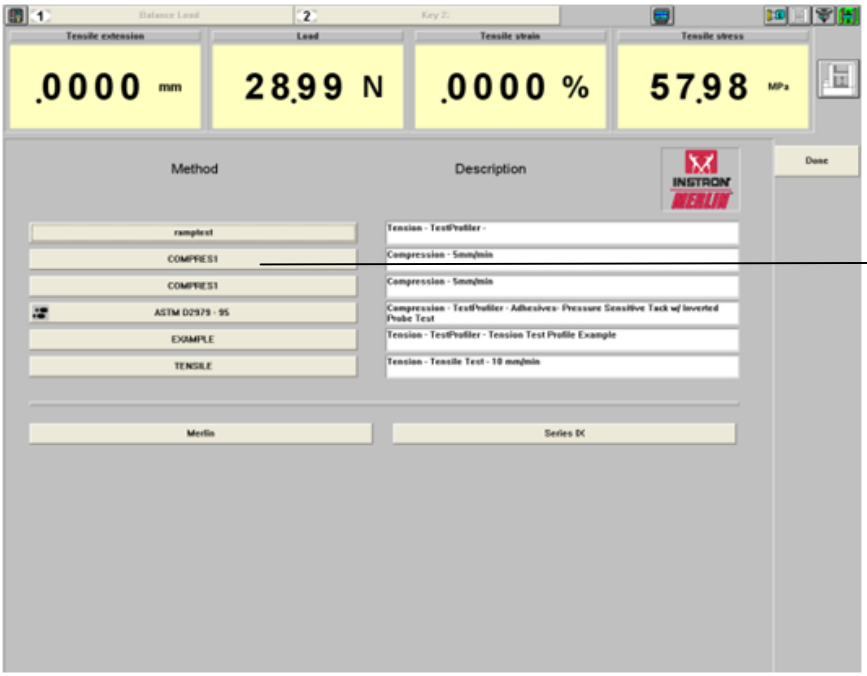

Sample Test Icon

Step 2:

- On clicking the respective sample test (tensile, compression, ramp test) icon in the main menu the following window appears on the screen which is the main window for the test.
- Click the test control button on the right side of the screen to open the test profiler window

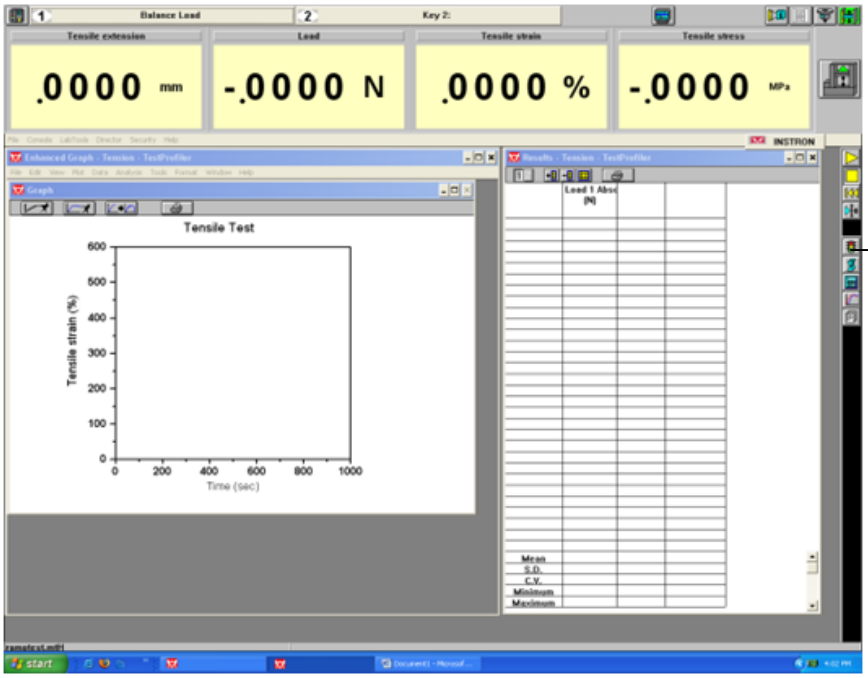

Test Control Button

Step 3:

- Upon clicking the test control button the test profile pop up window opens up on the screen.
- Click on the test button and then the profiler button to open the actual test set up window.

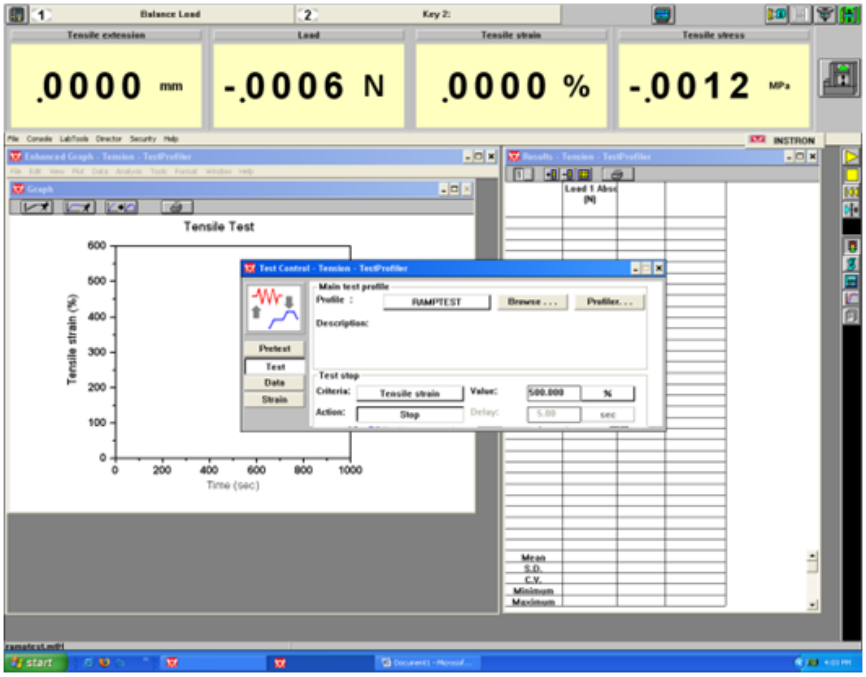

Step 4:

- The following test set up window allows the user to modify the rate of the loading of the ramp input, the time of relaxation as well as the amount of tensile strain applied to the material in each ramp

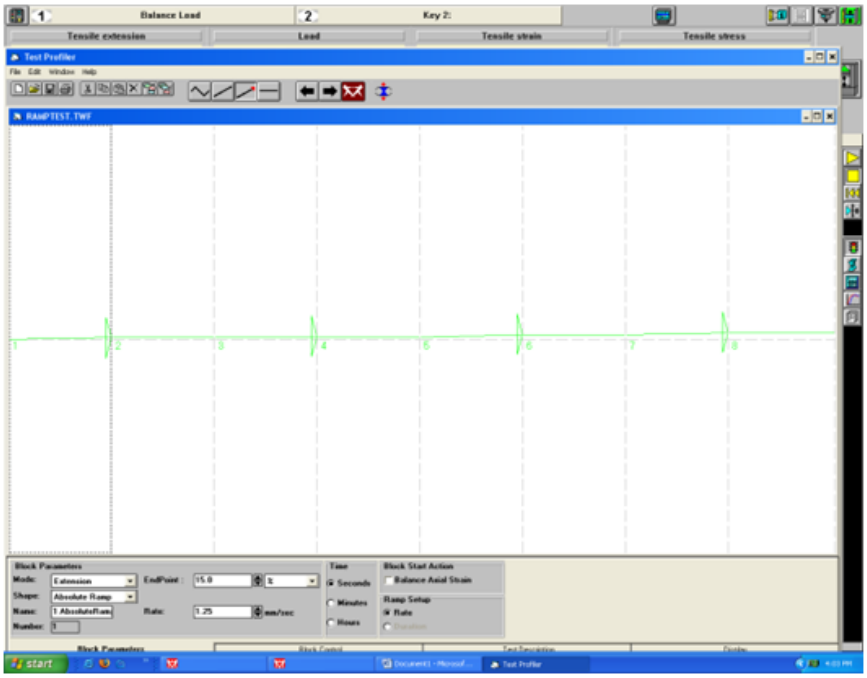

.

Step 5:

- To set up the first ramp, select the extension mode from the dropdown Mode menu.

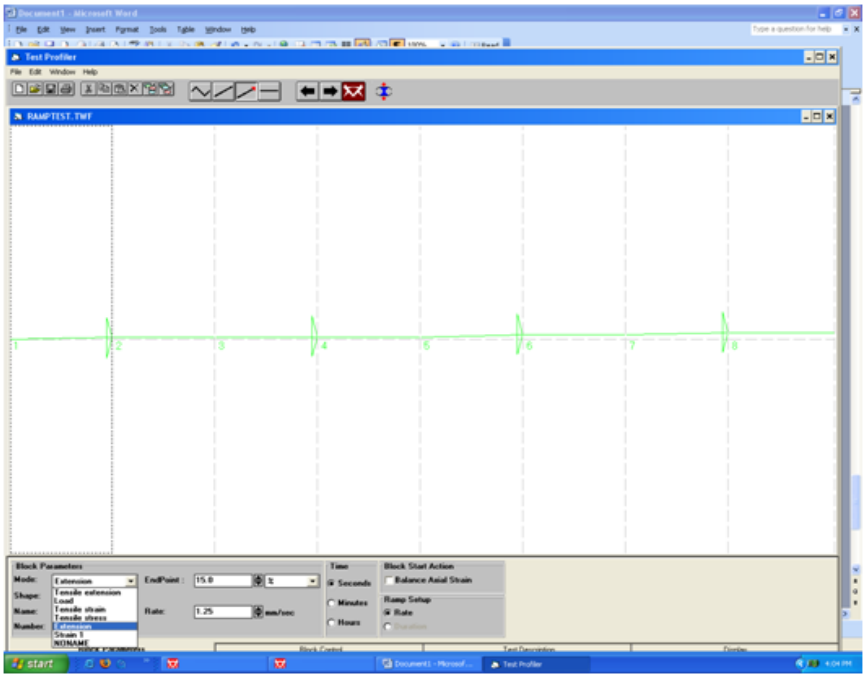

Step 6:

- From the Shape drop down menu select the absolute ramp mode.

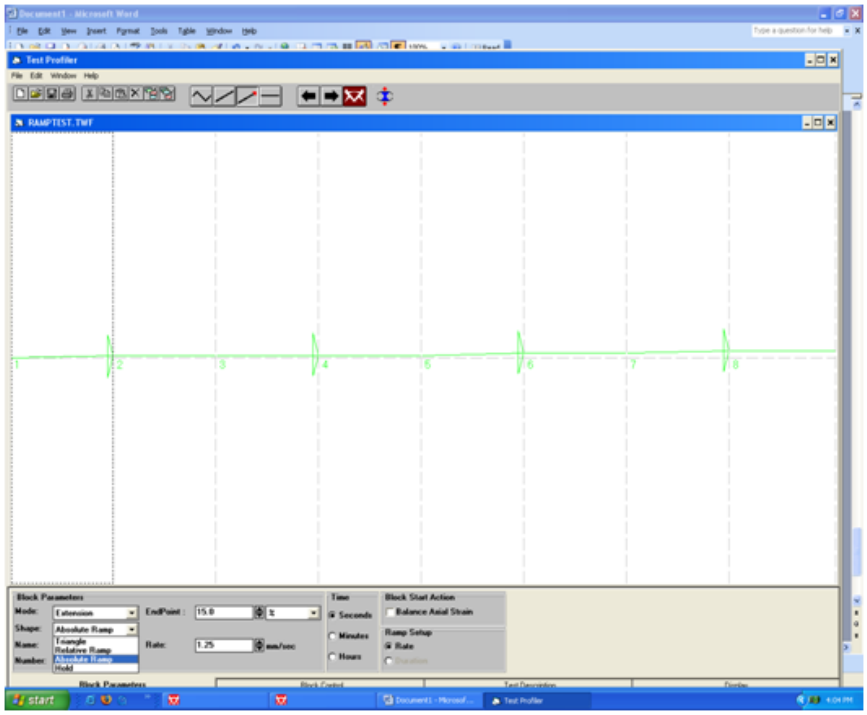

Step 7:

- Select the desired value of strain as the end point for the first ramp and select the desired unit for the strain (mm/mm or %).
- Also input the desire strain rate value and unit.

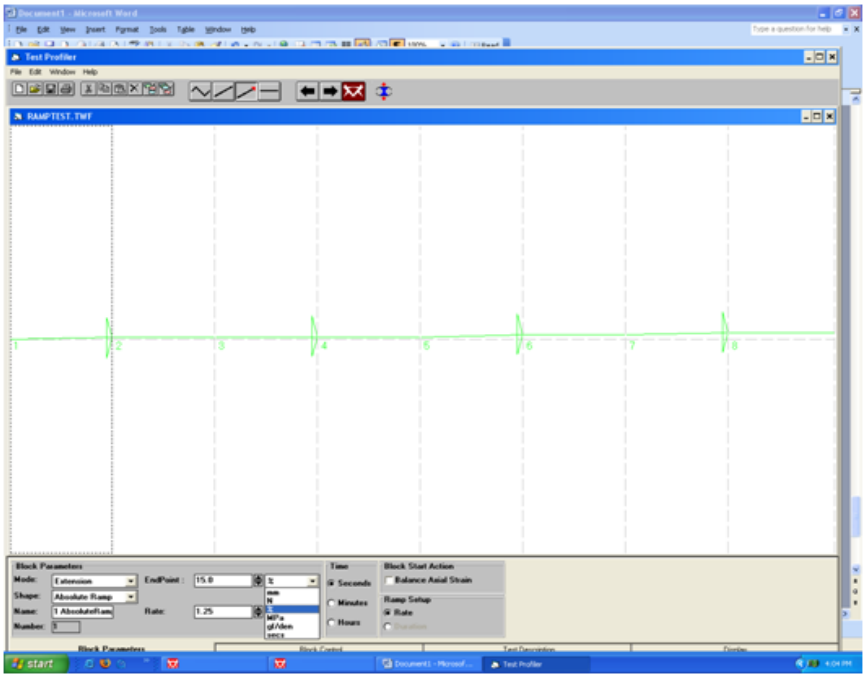

Step 8:

- For the relaxation part select the hold mode from the dropdown list in the Mode menu.

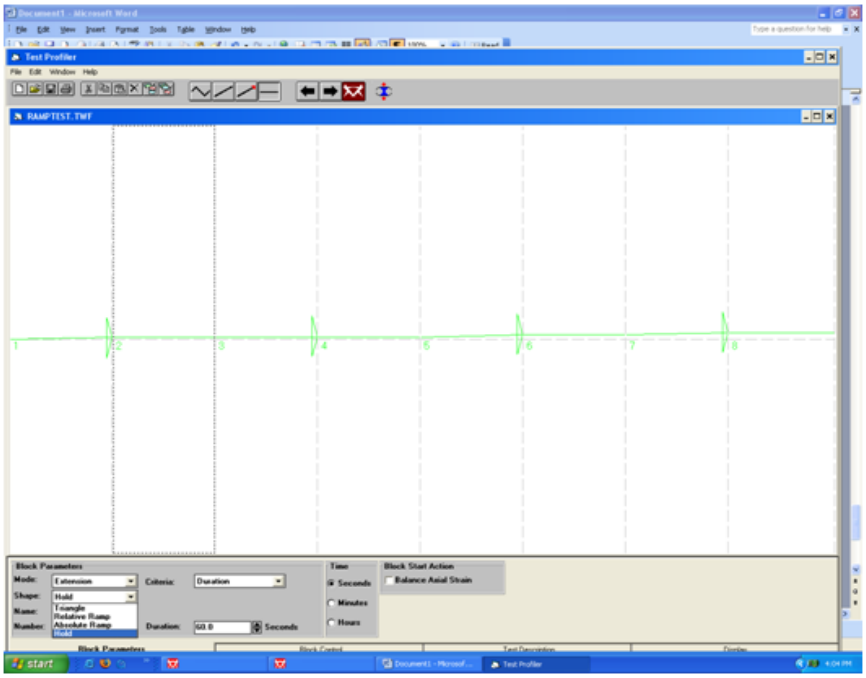

Step 9:

- Select the criterion as duration and input the amount of time duration for the relaxation time (60, 100 or 200 s).
- Repeat the same procedure 4 imes for four successive cycles of “ramp and hold” type.

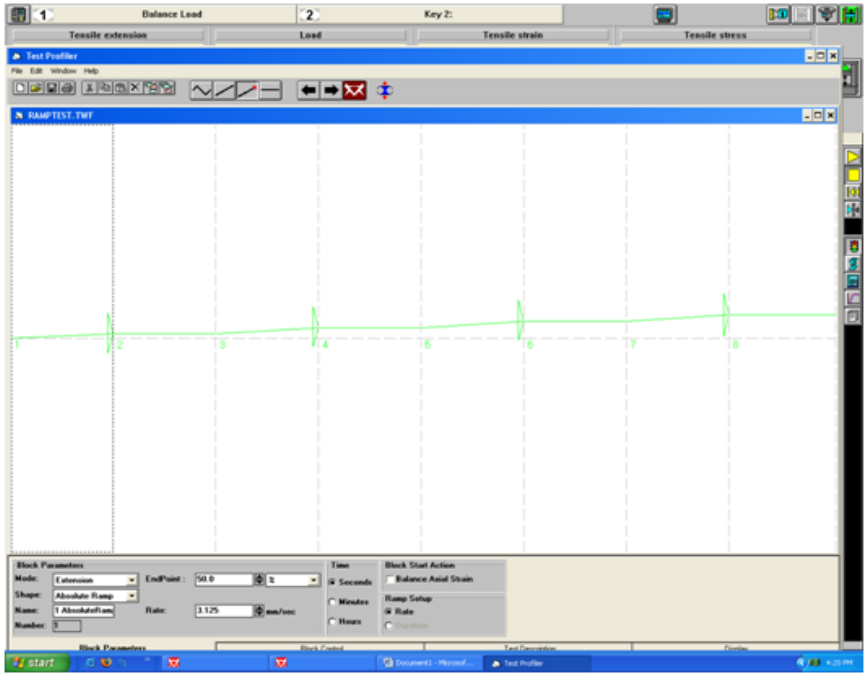

Step 10:

- To save the testing method, select the save as button in the file menu and save the test by giving it a desired name.

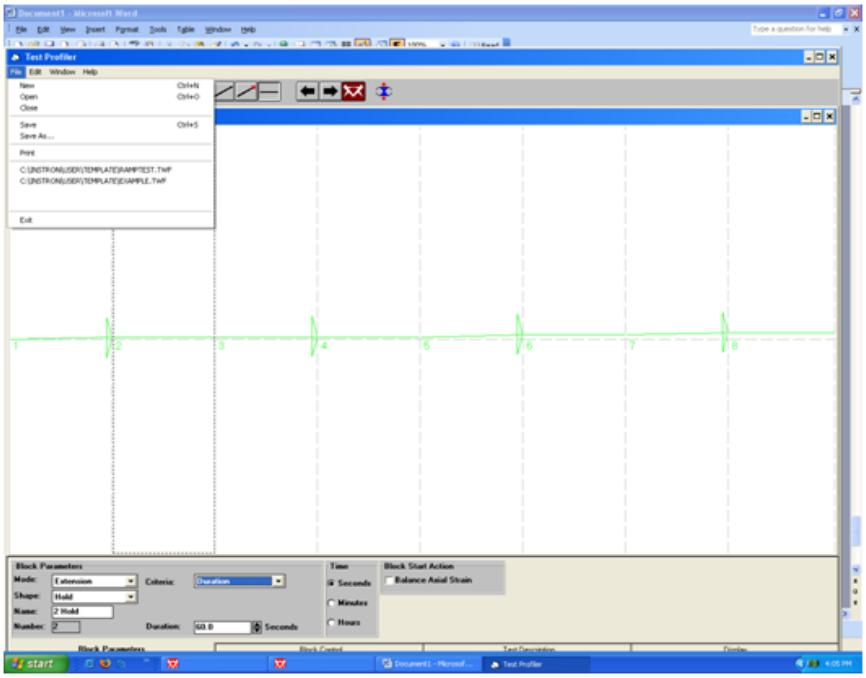

STEPS TO PERFORM THE TEST

Step 1:

- Click the button on the main test window to open the pop up box.
- Click the define button in this box to enter the name, geometry and number of specimens to be tested.

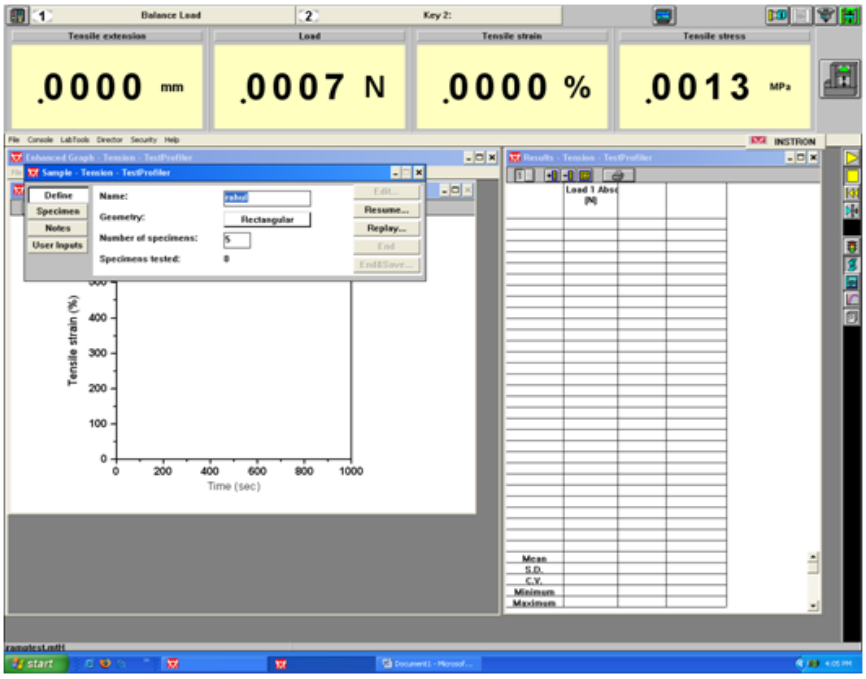

Step 2:

- Once this information had been entered then click the specimen button to enter the specimen specifications.

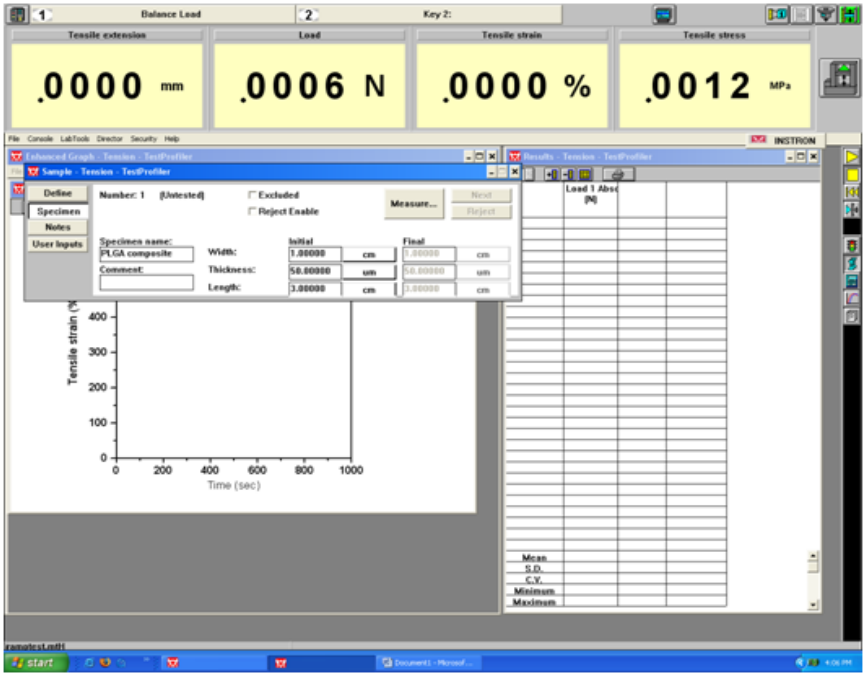

Step 3:

- Fix the specimen in the grips provided and reset the gauge length to zero using the reset gauge length button on the console.
- Then click the balance load button to set the load value on the specimen as zero.
- Click the yellow start test button on the screen to start the test.
- The strain vs. time curve for the stress relaxation test is as shown.

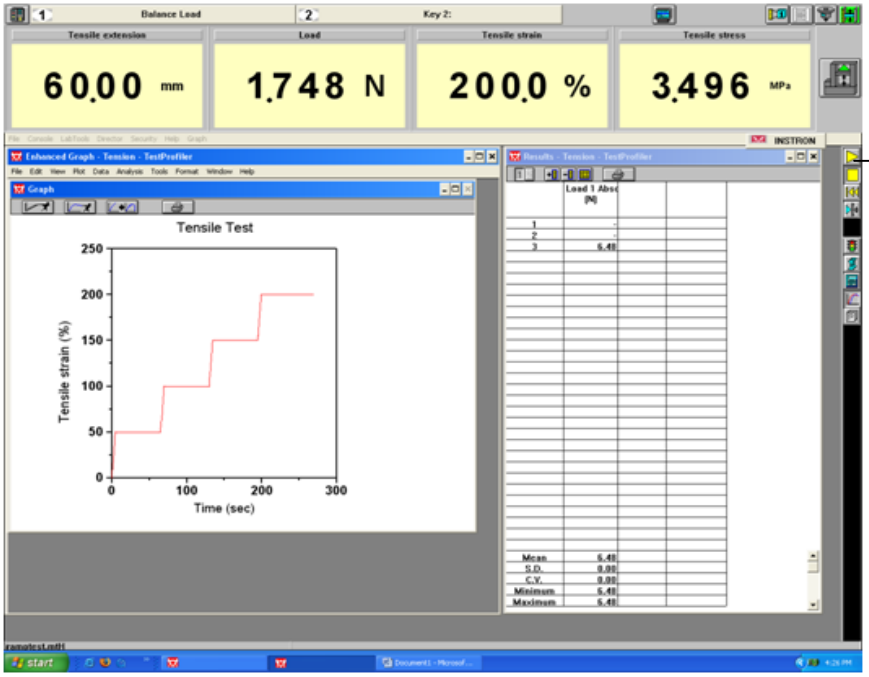

Step 4:

- The resultant output stress vs. time curve for the stress relaxation experiment with the previous successively increasing constant rate ramp input of strain is as shown.

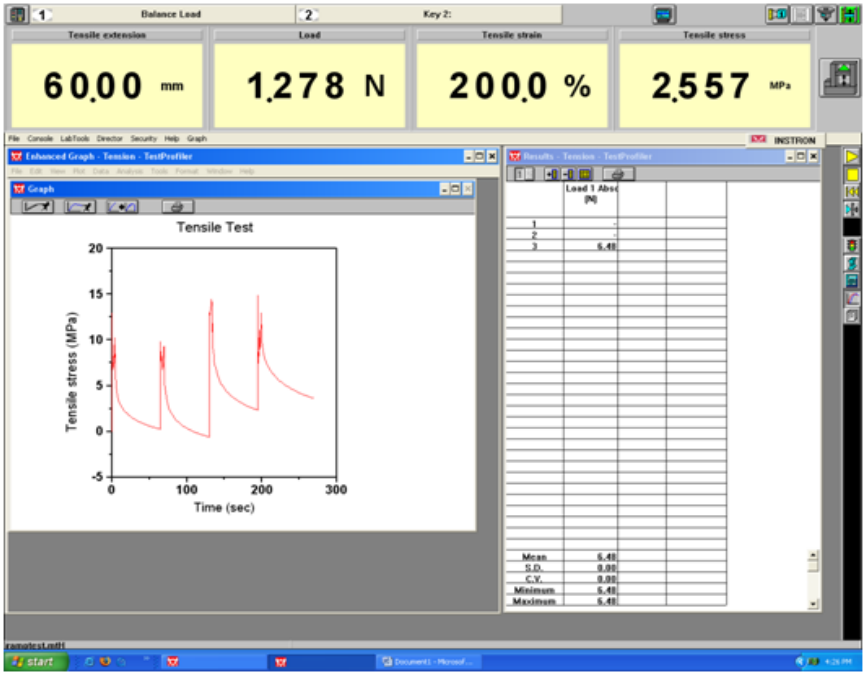

Step 5:

- To save the data for the test open the file menu from the upper toolbar and select End & Save in the drop down Data menu.

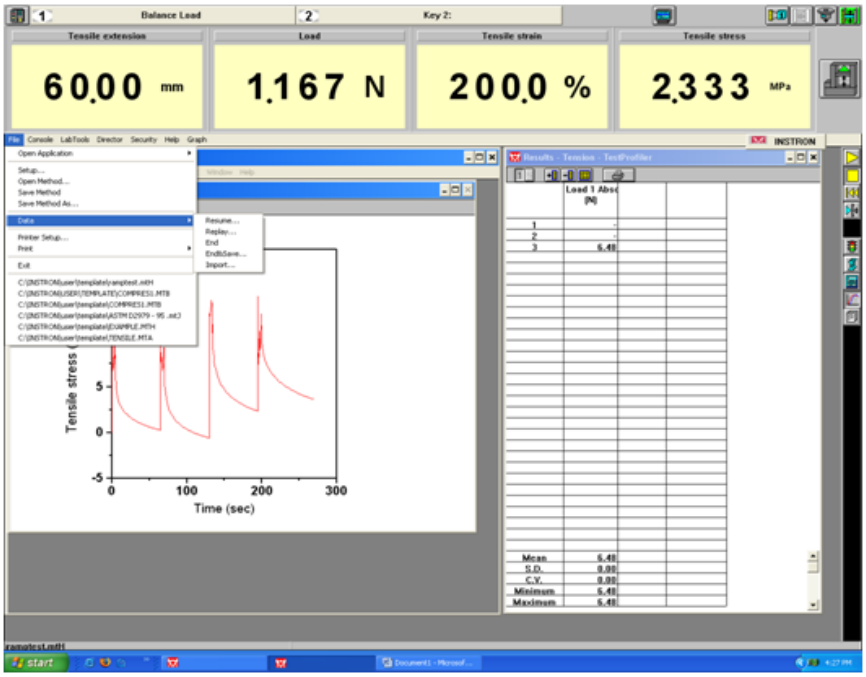

Step 6:

- Save data as a .RAW file with the desired file name.

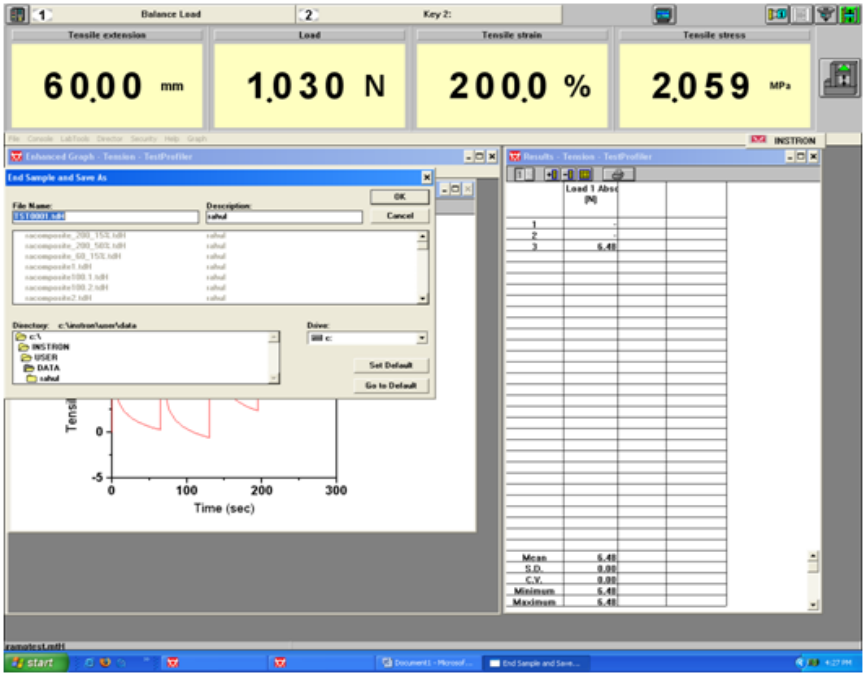

APPENDIX 2

ANALYTICAL MODEL DERIVATION

The QLV theory assumes that the stress relaxation behavior of soft tissues can be expressed as

$$\sigma(\varepsilon,t) = G(t)\sigma^e(\varepsilon(\tau)) \tag{A.1}$$

where $\sigma^e(\varepsilon(\tau))$ is the instantaneous elastic response i.e. the maximum stress in response to an instantaneous step input of strain ε.

G(t) is the reduced relaxation function that represents the time dependent stress response of the tissue normalized by the stress at the time of the step input of strain i.e.

$$G(t) = \frac{\sigma(t)}{\sigma(0^+)}, G(0^+) = 1$$

According to [85] the stress at any time t, $\sigma(\varepsilon,t)$ is given by the convolution integral of the strain history and G(t)

$$\sigma(\varepsilon,t) = \int_{-\infty}^{t} G(t-\tau)\frac{\partial\sigma^e(\varepsilon(\tau))}{\partial\varepsilon}\frac{\partial\varepsilon(\tau)}{\partial\tau}d\tau \tag{A.2}$$

In our case the applied stain history begins from time t=0, thus the equation modifies to

$$\sigma(\varepsilon,t) = \int_{0}^{t} G(t-\tau)\frac{\partial\sigma^e(\varepsilon(\tau))}{\partial\varepsilon}\frac{\partial\varepsilon(\tau)}{\partial\tau}d\tau \tag{A.3}$$

Fung [85] proposed the following generalized reduced relaxation function equation for G(t) based upon a continuous spectrum of relaxation

$$G(t)=\left[\frac{1+\int_0^{\infty} S(\tau)e^{-t/\tau}d\tau}{1+\int_0^{\infty} S(\tau)d\tau}\right] \tag{A.4}$$

where S(τ) is a continuous spectrum and has the following special form

$$\begin{aligned} S(\tau)&=\frac{C}{\tau} \text{ for } \tau_1<\tau<\tau_2 \\ &=0 \text{ for } \tau<\tau_1, \tau>\tau_2 \end{aligned} \tag{A.5}$$

Eq.(A.4) can be rewritten as

$$G(t)=\frac{1+C\left[E_1\left(t/\tau_2\right)-E_1\left(t/\tau_1\right)\right]}{1+C\ln\left(\tau_2/\tau_1\right)} \tag{A.6}$$

Where E_1 is the exponential function and has a form of

$$E_1(t/\tau)=\int_{t/\tau}^{\infty}\frac{e^{-z}}{z}dz \tag{A.7}$$

C, τ_1 and τ_2 are material constants to be determined

If τ_1 and τ_2 differ sufficiently that $\tau_1 << t << \tau_2$, then Eq.(A.6) can be written [30] as

$$G(t)=\frac{1-C\gamma-C\ln\left(t/\tau_2\right)}{1+C\ln\left(\tau_2/\tau_1\right)}+0(C) \tag{A.8}$$

Where γ is the Euler constant which has a value of 0.5772 and O(C) is small and can be neglected

Thus

$$G(t-\tau)=\frac{1-C\gamma-C\ln\left(\frac{t-\tau}{\tau_2}\right)}{1+C\ln\left(\tau_2/\tau_1\right)} \tag{A.9}$$

The commonly accepted [25, 30] instantaneous elastic response is given by an exponential approximation

$$\sigma^e(\varepsilon)=A\left(e^{B\varepsilon}-1\right) \tag{A.10}$$

Thus

$$\frac{\partial\sigma^e(\varepsilon)}{\partial\varepsilon}=ABe^{B\varepsilon} \text{ and } \frac{\partial\varepsilon}{\partial\tau}=\alpha$$

where α is the constant strain rate of loading. Thus Eq.(A.3) now becomes

$$\sigma(t)=\int_0^t G(t-\tau)ABe^{B\varepsilon}\alpha d\tau$$

Substituting $G(t-\tau)$ from equation (A.9) yields

$$\sigma(t)=\int_0^t ABe^{B\varepsilon}\alpha\frac{1-C\gamma-C\ln\left(\frac{t-\tau}{\tau_2}\right)}{1+C\ln\left(\tau_2/\tau_1\right)}d\tau \tag{A.11}$$

For a period of constant strain rate[25], α, $\varepsilon=\alpha\tau$

Taking the constant terms out of the integral in Eq.(A.11)

$$\sigma(t)=\frac{AB\alpha}{1+C\ln\left(\tau_2/\tau_1\right)}\int_0^t e^{B\alpha\tau}\left[1-C\gamma-C\ln\left(\frac{t-\tau}{\tau_2}\right)\right]d\tau \tag{A.12}$$

Applying the distributive property of multiplication

$$\sigma(t)=\frac{AB\alpha}{1+C\ln\left(\tau_2/\tau_1\right)}\int_0^t\left[e^{B\alpha\tau}-C\gamma e^{B\alpha\tau}-Ce^{B\alpha\tau}\ln\left(\frac{t-\tau}{\tau_2}\right)\right]d\tau \tag{A.13}$$

Integrating simple terms

$$\sigma(t)=\frac{AB\alpha}{1+C\ln\left(\tau_2/\tau_1\right)}\left[\frac{e^{B\alpha\tau}-1}{B\alpha}-\frac{C\gamma}{B\alpha}\left(e^{B\alpha\tau}-1\right)-C\int_0^t\left[e^{B\alpha\tau}\ln\left(\frac{t-\tau}{\tau_2}\right)\right]d\tau\right] \tag{A.14}$$

Let the integral in Eq.(A.14) be represented as I_1, i.e., $I_1=\int_0^t\left[e^{B\alpha\tau}\ln\left(\frac{t-\tau}{\tau_2}\right)\right]d\tau$

Using a variable transformation, $X=\left(\frac{t-\tau}{\tau_2}\right)$, then

$$I_1=\tau_2 e^{B\alpha t}\int_0^{t/\tau_2} e^{-B\alpha\tau_2 X}\ln X dX \tag{A.15}$$

with substitution $B\alpha\tau_2=Z$

$$I_1=\tau_2 e^{B\alpha t}\int_0^{t/\tau_2} e^{-ZX}\ln X dX$$

Using integration by parts with *ln X* and $e^{-ZX}dX$ as individual terms,

$$I_1=\tau_2 e^{B\alpha t}\left[\frac{e^{-ZX}}{-Z}\ln X\Big|_0^{t/\tau_2}-\int_0^{t/\tau_2}\frac{e^{-ZX}}{-ZX}dX\right]$$

Or $I_1 = \tau_2 e^{B\alpha t}\left[\frac{1}{-Z}\right]\left[e^{-ZX}\ln X\Big|_0^{t/\tau_2} - \int_0^{t/\tau_2}\frac{e^{-ZX}}{ZX}ZdX\right]$ (A.16)

Let the integral in Eq.(A.16) be represented as I_2 i.e., $I_2 = \int_0^{t/\tau_2}\frac{e^{-ZX}}{ZX}ZdX$

Using Y=ZX as a variable transformation to

$$I_2 = \int_0^{B\alpha t}\frac{e^{-Y}}{Y}dY = \int_0^{\infty}\frac{e^{-Y}}{Y}dY - \int_{B\alpha t}^{\infty}\frac{e^{-Y}}{Y}dY \quad \text{(A.17)}$$

From [95] $E_1(Y) = \int_Y^{\infty}\frac{e^{-Y}}{Y}dY$ where

$$E_1(Y) = -\gamma - \ln Y - \sum_{k=1}^{\infty}\frac{(-1)^k Y^k}{kk!}\quad |Arg(Y)| < \pi \quad \text{(A.18)}$$

Then $I_2 = E_1(0) - E_1(B\alpha t) = -E_1(Y)\Big|_0^{B\alpha t}$

Substituting into Eq.(A.16)

$$I_1 = \tau_2 e^{B\alpha t}\left[\frac{1}{-Z}\right]\left[e^{-ZX}\ln X\Big|_0^{t/\tau_2} + E_1(Y)\Big|_o^{B\alpha t}\right] \quad \text{(A.19)}$$

Substituting Eq.(A.18) for $E_1(Y)$

$$I_1 = \tau_2 e^{B\alpha t}\left[\frac{1}{-Z}\right]\left[e^{-ZX}\ln X\Big|_0^{t/\tau_2} - \left[\gamma + \ln Y + \sum_{k=1}^{\infty}\frac{(-1)^k Y^k}{kk!}\right]_o^{B\alpha t}\right] \quad \text{(A.20)}$$

Using ε for the lower limit and substituting the limits of integration

$$I_1 = \tau_2 e^{B\alpha t}\left[\frac{1}{-B\alpha\tau_2}\right]\left[e^{-B\alpha t}\ln\left(\frac{t}{\tau_2}\right) - e^{-B\alpha\tau_2\varepsilon}\ln\varepsilon - \left[\gamma + \ln B\alpha t + \sum_{k=1}^{\infty}\frac{(-1)^k(B\alpha t)^k}{kk!} - \gamma - \ln\varepsilon - \sum_{k=1}^{\infty}\frac{(-1)^k\varepsilon^k}{kk!}\right]\right] \quad \text{(A.21)}$$

As ε →0

$$\lim_{\varepsilon\to 0}\sum_{k=1}^{\infty}\frac{(-1)^k\varepsilon^k}{kk!} \approx 0$$

Grouping terms with lnε and using L'Hoptal's rule

$$\lim_{\varepsilon\to 0}(1 - e^{-B\alpha\tau_2\varepsilon})\ln\varepsilon \approx 0$$

Then Eq.(A.21) reduces to

$$I_1 = \frac{-e^{B\alpha t}}{B\alpha}\left[e^{-B\alpha t}\ln\left(\frac{t}{\tau_2}\right) - \ln B\alpha t - \sum_{k=1}^{\infty}\frac{(-1)^k(B\alpha t)^k}{kk!}\right] \quad \text{(A.22)}$$

Inserting I_1 into Eq. (A.14)

$$\sigma(t) = \frac{AB\alpha}{1 + C\ln(\tau_2/\tau_1)}\left[\frac{e^{B\alpha\tau} - 1}{B\alpha} - \frac{C\gamma}{B\alpha}\left(e^{B\alpha\tau} - 1\right) + \frac{Ce^{B\alpha t}}{B\alpha}\left[e^{-B\alpha t}\ln\left(\frac{t}{\tau_2}\right) - \ln B\alpha t - \sum_{k=1}^{\infty}\frac{(-1)^k(B\alpha t)^k}{kk!}\right]\right] \quad \text{(A.23)}$$

For the loading region $\sigma(0 < t \le t_0)$

$$\sigma(0 < t \le t_0) = \frac{A}{(1 + C\ln(\tau_2/\tau_1)}\left[\left(e^{B\alpha t} - 1\right)(1 - C\gamma) + C\ln\left(\frac{t}{\tau_2}\right) - Ce^{B\alpha t}\ln(B\alpha t) + Ce^{B\alpha t}\sum_{k=1}^{\infty}\frac{(-1)^k(B\alpha t)^k}{kk!}\right] \quad \text{(A.24)}$$

Solving similarly for the relaxation part

$$\sigma(t \geq t_0) = \frac{A}{(1+C\ln(\tau_2/\tau_1)}\Big[\left(e^{B\alpha t_0}-1\right)(1-C\gamma)+C\ln\left(\frac{t}{\tau_2}\right)-Ce^{B\alpha t_0}\ln\left(\frac{t-t_0}{\tau_2}\right)$$
$$-Ce^{B\alpha t}\ln\left(\frac{t-t_0}{\tau_2}\right)+Ce^{B\alpha t}\sum_{k=1}^{\infty}\frac{(-1)^k(B\alpha t)^k}{kk!}-Ce^{B\alpha t}\sum_{k=1}^{\infty}\frac{(-1)^k(B\alpha(t-t_0))^k}{kk!} \quad \text{(A.25)}$$

APPENDIX 3

OPTIMIZATION ALGORITHM

Step 1: Initialize

Randomize the starting point $\underline{x}_0$ (the Decision Variable initial trial solution, and best so far, the base value), and

Evaluate $f_0 = f(\underline{x}_0)$ (the Objection Function base value, and best so far)

Set $\underline{x} = \underline{x}_0$ (the trial solution is initialized as the base value)

Randomize the initial increments $\Delta^{(k)}$ for k = 1,2,3,…, N

(N = number of decision variables)

Choose the expansion factor (Expand_factor) (1.25 is a useful value)

Choose the contraction factor (Contract_factor) (0.8 is a useful value)

Step 2: Cycle through each Decision Variable (k=1, 2, … N) one-by-one, individually testing each new trial solution

$x^{(k)} = x_0{}^{(k)} + \Delta^{(k)}$ (create a new trial solution value for the k^{th} decision variable)

Evaluate $f = f(\underline{x})$ (the Objection Function value with the new $x^{(k)}$ value.

Step 3: Was $\underline{x}$ better than $\underline{x}_0$?

If Yes (defined here as $f < f_0$) Then

$x_0^{(k)} = x^{(k)}$ (accept new value as base value of k^{th} decision variable)

$\Delta^{(k)} = \Delta^{(k)} *$ Expand_factor (expand step size for next trial of k^{th} variable)

$f_0 = f$ (accept new OF value as the current best)

Else

$x^{(k)} = x_0^{(k)}$ (return the new trial value to the previous best for the k^{th} DV)

$\Delta^{(k+1)} = -\Delta^{(k)} *$ Contract_factor (reverse and contract k^{th} DV step size)

Return to Step 2 until each DV has been explored

Step 4: Check for termination

If termination criteria are satisfied, Then

Stop (current point approximates the optimum, $\underline{x}^*$)

Else

Return to Step 2 to begin a new cycle through each DV

VITA

Rahul Mirani

Candidate for the Degree of

Master of Science

Thesis: STRESS RELAXATION MODELING OF COMPOSITE POROUS SCAFFOLDS

Major Field: Chemical Engineering

Biographical:

Personal Data: Born on March 10, 1985

Education: Completed Bachelor of Engineering in Chemical Engineering from Nirma Institute of Technology, affiliated to Gujarat University, Ahmedabad, Gujarat, India. Completed the requirements for the Master of Science in Chemical Engineering at Oklahoma State University, Stillwater, Oklahoma in December, 2009

Experience: Working as Research Assistant from August 2007 to present
Working as Teaching Assistant for Advanced Chemical Engineering Modeling from August 2009 to present
Worked as a Teaching Assistant for Computer Programming, Visual Basic for Application from January 2009 to May 2009
Worked as teaching Assistant for Chemical Engineering Thermodynamics from August 2007 to December 2007
Worked as a Process Engineer at Reliance Industries limited, India from September 2006 to July 2007

Professional Memberships:
Chemical Engineering Student Association (ChESA) 2002-2006
(Nirma Chapter, Ahmedabad, India)
American Institute of Chemical Engineers (AIChE) 2008-2009

Name: Rahul Mirani Date of Degree: December, 2009

Institution: Oklahoma State University Location: Stillwater, Oklahoma

Title of Study: STRESS RELAXATION MODELING OF COMPOSITE POROUS SCAFFOLDS

Pages in Study: 85 Candidate for the Degree of Master of Science
Major Field: Chemical Engineering

Scope and Method of Study: The objective of this study was to evaluate the viscoelastic characteristics of potential scaffolds to be used in tissue regeneration. PLGA based composite scaffold was used as a model structure for evaluating viscoelastic stress relaxation characteristics by performing experiments of the "Ramp-and-Hold" type. Quasi Linear Viscoelastic (QLV) model, the most widely used model in biomechanics, was used to quantify the viscoelastic behavior of the scaffold in terms of the physiological model parameters. Also, the viscoelastic characteristics of the composite scaffold were evaluated in tandem with the natural matrix SIS.

Findings and Conclusions: "Ramp-and-Hold" experimental results showed that the PLGA composite structure relaxes better than SIS. This was in concurrence with the values of the phenomenological QLV model parameters. Also, the PLGA composite was found to be strain rate softening compared to the strain rate hardening of SIS. Curve-fitting results revealed that the model successfully predicted the experimental data for SIS with less than 2% relative error. For the PLGA composite, though the model correctly predicted the trend observed in the experimental data, it failed to fit the data correctly. This can be attributed to the numerous assumptions involved in the derivation of the QLV model. This warrants the need for a robust, phenomenological model based purely on the material behavior devoid of assumptions for assessing the viscoelastic properties of synthetic scaffolds.

ADVISER'S APPROVAL: Dr. Sundararajan V. Madihally